Human CD4/CD8 double positive T cells are both predictive and sufficient to mediate GVHD pathology

Nicholas J. Hess[1,2], David Turicek[1], Jeremiah Riendeau[3,4], Sean J. McIlwain[5], Emmanuel Contreras Guzman[3,4], Kalyan Nadiminti[2,8], Amy Hudson[6], Natalie Callander[2], Melissa C. Skala[3,4], Jenny E. Gumperz[7,8], Peiman Hematti[2,8], *Christian M. Capitini[1,8]

[1]Department of Pediatrics, University of Wisconsin School of Medicine and Public Health, Madison, WI

[2]Division of Hematology/Oncology, Department of Medicine, University of Wisconsin School of Medicine and Public Health, Madison, WI

[3]Morgridge Institute for Research, Madison, WI

[4]Department of Biomedical Engineering, University of Wisconsin-Madison, Madison, WI

[5]Department of Biostatistics and Medical Informatics, University of Wisconsin-Madison, Madison, WI

[6]Department of Microbiology and Immunology, Medical College of Wisconsin, Milwaukee, WI

[7]Department of Medical Microbiology and Immunology, University of Wisconsin School of Medicine and Public Health, Madison, WI

[8]University of Wisconsin Carbone Cancer Center, Madison, WI

***Corresponding Author**:

Christian M. Capitini

University of Wisconsin School of Medicine and Public Health

WIMR 4137, 1111 Highland Ave

Madison, WI 53705

Office: (608) 262-2415

Fax: (608) 265-9721

Email: ccapitini@pediatrics.wisc.edu

ORCID: 0000-0001-5720-9305 (NJH); 0000-0003-1852-2192 (JG)

Abstract Word Count = 190

Word Count = 9704

Reference Count = 58

Running Title: DPTs Are Predictive and Sufficient for GVHD

Abstract

An important paradigm to improve allogeneic hematopoietic stem cell transplantations (allo-HSCTs) is the prevention of graft-vs-host disease (GVHD) while preserving the beneficial graft-vs-leukemia (GVL) activity of donor T cells. In an observational clinical study of adult allo-HSCT recipients, we identified five T cell specific predictive biomarkers of relapse and GVHD. One interesting biomarker was the emergence of a CD4/CD8 double positive T cell (DPT) population not present in the starting graft tissue. Using a xenogeneic transplant model, we reveal that DPTs are predictive of lethal GVHD irrespective of donor or graft source. We observed that DPTs originated from the CD8 T cell population, co-expressed both RUNX3 and THPOK and are not a by-product of a lymphopenic environment. Transcriptomic, metabolomic and functional assays all revealed DPTs to be a highly activated T cell population distinct from both CD4 and CD8 T cells. Importantly, DPTs isolated from GVHD mice were sufficient to mediate xenogeneic GVHD after re-transplantation but had no observable GVL activity when challenged in vivo with two human B-ALL malignancies. Overall, these studies highlight a GVHD-specific human T cell population with the potential to delineate GVL activity from GVHD pathology.

Introduction

Graft-vs-host disease (GVHD) and relapse remain the primary complications following allogeneic hematopoietic stem cell transplantation (allo-HSCT)[1–3]. While the field has made significant strides in reducing GVHD, current GVHD prophylaxis drug regimens target the entire T cell population, potentially hindering the efficacy of graft-vs-leukemia (GVL) activity mediated by donor T cells[4–8]. Thus, identifying predictive biomarkers and delineating specific cellular mechanism(s) leading to GVHD pathology versus GVL activity has remained a top priority for the field.

Unfortunately, separating the graft-vs-host (GVH) response of donor T cells from their GVL activity has proven difficult as both responses are derived from allogeneic antigen stimulation[7–9]. Nevertheless, several studies have investigated the role of specific HLA mismatches on the development of GVHD and GVL activity[10–13]. These studies have highlighted the importance of permissive and non-permissive HLA mismatches on GVHD development and non-relapse mortality, but correlating them with GVL activity has been met with limited success[10–14]. Furthermore, the use of haploidentical transplantations with post-transplant cyclophosphamide has shown that HLA matching of the donor and recipient may not play a dominant role in separating GVH and GVL activity[15,16].

While pre-transplant prognostic variables such as HLA-matching, conditioning regimens and graft source all influence allo-HSCT outcomes, these population-based variables are not able to predict individual patient outcomes[17–19]. Several post-transplant predictive variables have been discovered including sST2, REG3α, elafin and others[20–26]. These highly promising plasma-based biomarkers are generally released due to host damage and have shown efficacy in predicting the development of steroid-resistant GVHD and non-relapse mortality (NRM) either individually or combined into a predictive algorithm[20–26]. To date though, these biomarkers have not been able to predict an allo-HSCT recipients' chance of relapse as they measure the degree of host damage

77 rather than donor T cell alloreactivity.

78

79 While all the validated GVHD biomarkers to date have been plasma-based, the direct
80 investigation of T cell subsets as biomarkers has been another area of active investigation[27–30].
81 Both CD4 and CD8 T cells can respond to allogeneic antigens, but while CD8 T cell may be
82 directly responsible for cellular cytotoxicity, CD4 T cells have recently been the primary focus of
83 the field[31–33]. The CD4 population is unique in its capacity to polarize into a variety of different
84 subsets, based on the cytokine environment it finds itself, to drive an inflammatory response[34–40].
85 In the case of GVHD, TH_1 and $TH_{17/22}$ cells have been shown to be directly involved in driving the
86 pathogenesis of gastrointestinal, liver and skin pathology[35,41]. In contrast, the CD8 T cell
87 population is thought to be fairly uniform in their role as cytotoxic effectors licensed by CD4 T
88 cells. The discovery of CD8 regulatory T cells in murine GVHD though suggests CD8 T cells may
89 also be able to polarize into different subsets similar to the CD4 population[42,43]. Despite our
90 increased understanding of GVHD pathogenesis mediated allo-reactive T cells, T cell specific
91 GVHD prophylaxis regimens (e.g. ATG, abatacept) have been slow to enter the clinic and have
92 not yet shown a direct cellular mechanism separating GVH from GVL activity.

93

94 Interestingly, several recent studies have now identified a novel human T cell population co-
95 expressing both CD4 and CD8 lineage markers in a variety of chronic inflammatory diseases,
96 including GVHD[44–51]. Historically, CD4/CD8 double positive T cells (DPTs) have only existed as
97 a developmental stage of T cells in the thymus that are unable to survive in the periphery due to
98 the lack of survival signals[52,53]. The presence of DPTs in the periphery of these human chronic
99 inflammatory diseases suggests either a breakdown in T cell development or that DPTs in the
100 periphery are a previously unidentified mature human T cell population with an unknown origin
101 and function[53].

102

103 In this study, we identify five T cell metrics capable of predicting relapse, GVHD or both in allo-
104 HSCT recipients several weeks to months prior to their diagnosis. One of these predictive
105 biomarkers was the frequency of DPTs which we explored further in a xenogeneic transplant
106 model. This xenogeneic transplant model was able to successfully recapitulate the development
107 and predictive potential of DPTs with lethal xenogeneic GVHD. We also reveal that DPTs alone
108 are sufficient to mediate GVHD pathology but have little GVL activity against two human B-ALL
109 cancer lines. This study also identifies the origin of DPTs as the CD8 T cell population. Overall,
110 this study describes the origin and function of a novel human T cell population that has clinical
111 significance in its ability to predict GVHD in allo-HSCT recipients and is sufficient for GVHD
112 pathology but not GVL activity in a xenogeneic transplant model.
113
114 **Results**
115
116 **T cell specific predictive biomarkers of relapse and GVHD in allo-HSCT recipients**
117 To determine if the direct measurement of T cells in allo-HSCT recipients post-transplant can
118 serve as predictive biomarkers of relapse and/or GVHD, we collected 417 blood samples from 35
119 adult allo-HSCT recipients over their first 100 days post-transplant (Fig 1A). Patients were
120 included in the observational study irrespective of their conditioning regimen, donor HLA
121 matching, graft source or GVHD prophylaxis regimen with the only requirement being they
122 received post-transplant cyclophosphamide (Supplemental Table 1). Samples were processed
123 within seven days of collection and never frozen. Antigen-experienced T cells were gated based
124 on CD3 and CD45RO expression as a means to exclude non-reactive donor T cells and naïve T
125 cells that are present due to de novo hematopoiesis (Supplemental Fig 1).
126
127 From a total of 11 T cell metrics analyzed, we identified five metrics as having the capacity to
128 predict relapse, GVHD (of any grade) or ≥ grade 2 GVHD, the number of $CD45RO^{+}$ T cells and

129 frequency of blasting CD45RO$^+$ T cells, regulatory T cells (T_{regs}), CD8$^+$ T cells and DPTs (Fig 1B).
130 We first analyzed the samples collected between days 7 and 17 in three binary tests to determine
131 if any could significantly differentiate between two allo-HSCT outcomes. Tests that were shown
132 to be significant by t-test were further evaluated using a receiver-operator-characteristic (ROC)
133 analysis (Fig 1C). We identified two predictive biomarkers of relapse (CD45RO T cells and
134 frequency of Tregs), four predictive biomarkers of GVHD (CD45RO T cells and the frequency of
135 Tregs, CD8 and DPTs) and two predictive biomarkers of ≥ grade 2 GVHD (frequency of Tregs
136 and DPTs) (Fig 1C). Combining the individual T cell metrics into one multi-parameter analysis
137 further increased their predictive potential as measured by the area-under-the-curve (AUC) values
138 that reached 0.848, 0.736 and 0.701 for relapse, GVHD and ≥ grade 2 GVHD prediction
139 respectively (Fig 1D).
140
141 A second analysis included patient samples collected between days 22 and 83 and were further
142 normalized relative to each individual patient's date of low grade 1 or 2 GVHD diagnosis. For
143 patients who did not develop GVHD, we normalized their data to day 54, which was the average
144 time to GVHD diagnosis among our cohort. In this analysis, only three of the original five T cell
145 biomarkers showed any predictive value with all three metrics predicting relapse (CD45RO T cells
146 and the frequencies of CD8 and DPTs) and the frequency of CD8 and DPTs predicting both GVHD
147 (of any grade) and ≥ grade 2 GVHD (Fig 1E). Combining the predictive metrics into one multi-
148 parameter analysis as before further increase their predictive value with AUC values of 0.892,
149 0.741 and 0.734 for relapse, GVHD and ≥ grade 2 GVHD prediction respectively (Fig 1F).
150
151 **Xenogeneic transplantation also reveals DPTs as a predictive biomarker of GVHD**
152 **development**
153 To replicate our clinical observational study, we utilized a human xenogeneic transplant model
154 wherein we transplanted various human graft tissue into immunodeficient mice[31,54,55]. As in our

155 observational clinical study, we observed the presence of DPTs, which were not present in the
156 starting healthy graft tissue, primarily developing in mice that would later develop lethal
157 xenogeneic GVHD (Fig 2A). We confirmed that DPTs are not an artifact of doublets by
158 ImageStream analysis and develop even when isolated human T cells are used for transplantation
159 (Fig 2B and Supplemental Fig 2). DPTs were present in variety of GVHD target organs and
160 developed as early as 1wk after transplant in each of the four graft sources we tested (Fig 2C-H).
161 The increased frequency of DPTs was also a predictive biomarker of lethal GVHD development
162 in this model system at 1-, 3- and 6-weeks post-transplant (Fig 2I). We further confirmed that the
163 frequency of Tregs at 1-week after transplant could act as a predictive biomarker of lethal
164 xenogeneic GVHD but with the contribution of Tregs already well established in GVHD, we chose
165 to focus on the origin and function of DPTs for the remainder of this study (Supplemental Fig 3).
166
167 **The DPT population is distinct from CD4 and CD8 T cells**
168 Two alternative hypotheses against DPT being a unique T cell population is the possibility that
169 CD4 T cells co-expressing CD8α upon activation or that CD4 or CD8 T cells could co-express the
170 alternative lineage marker through trogocytosis. To determine if either of these are possible, we
171 first show that DPTs express both CD8α and CD8β, suggesting this population is not the result of
172 an activated CD4 T cell population (Supplemental Fig 4A-B). Furthermore, we flow-sorted DPTs
173 from GVHD mice and expanded them in vitro and/or transplanted them into a naïve mouse. In
174 both cases, the DPT population persisted even in the absence of single positive CD4 and CD8 T
175 cells suggesting that co-expression of the CD4 and CD8 lineage markers is sustained and not the
176 result of trogocytosis (Supplemental Fig 4C-F). Additionally, the DPT population does not appear
177 to be the result of a dead/dying T cell population due to high expression of the anti-apoptotic
178 protein BCL2 (Supplemental Fig 4G).
179
180 To explore if the CD4 and CD8 lineage markers are actually co-transcribed, we performed RNA-

181 seq on flow-sorted CD4, CD8 and DPTs from GVHD mice (Fig 3). Analysis of the transcriptome
182 from these cells revealed that DPTs express a transcriptional signature unique from CD4 or CD8
183 T cells (Fig 3A-B). Using a threshold of $p<0.01$ and a fold change of >10 to determine significance,
184 we reveal that DPTs differentially expressed 63 genes compared to CD4 and CD8 T cells (Fig
185 3A). Of the differentially expressed genes, we confirmed that both CD4 and CD8 are both
186 transcriptionally expressed in DPTs (Fig 3C-E). Interestingly, DPTs also appear to express
187 several genes normally associated with B cell biology, though the mechanism for this observation
188 requires further investigation (Fig 3E).
189
190 Using all 796 genes differentially expressed in the DPT:CD4 and DPT:CD8 comparisons, KEGG
191 BRITE functional hierarchical classification highlighted numerous differentially expressed genes
192 serving as enzymatic genes along with CD molecules commonly observed on T cells, exosome
193 machinery, transcription factors and cytokine/cytokine receptors (Supplemental Table 2). We also
194 surveyed 13 inflammatory and inhibitory co-receptors on the surface of CD4, CD8 and DPTs from
195 GVHD mice (Fig 4A-C, Supplemental Fig 5). Interestingly, DPT displayed intermediate expression
196 of CD27, OX40, PD-1 and LAG3 compared to CD4 and CD8 T cells analyzed from the blood or
197 spleen of GVHD mice (Fig 4A-C, Supplemental Fig 5). The expression of these markers was
198 further explored on the T cells from our observational clinical study (Fig 4D-L). While the
199 expression of these markers differed slightly, most likely due to differences in a murine versus
200 human host environment, DPTs still displayed an expression profile of a terminally differentiated
201 effector T cell population with little evidence of exhaustion (Fig 4D-L).
202
203 **DPTs differentiate from the CD8 T cell population and upregulate THPOK**
204 To identify the T cell population that gives rise to DPTs, we performed an unsupervised tSNE
205 clustering of human T cells from a xenogeneic GVHD mouse using a nine-color flow cytometry
206 panel (Fig 5A). This analysis, in addition to the global transcriptomic analysis, indicated that DPTs

207 cluster more closely with CD8 T cells than CD4 T cells. Thus, despite the well documented
208 plasticity of the CD4 lineage, our results suggest that DPTs may develop from the CD8 lineage
209 (Fig 3B, Fig 5A).
210
211 To test this hypothesis, we transplanted isolated CD4 or CD8 T cells from a healthy donor into
212 our xenogeneic transplant model. Elevated frequencies of DPTs were only observed in mice
213 transplanted with isolated CD8 T cells, indicating that mature CD8 T cells and not CD4 or
214 progenitor T cells give rise to the DPT population (Fig 5B-C). Clonal TCR analysis of the TRAB
215 gene within the CD4, CD8 and DPT populations also provide evidence that the CD4 and DPT
216 populations are experiencing clonal expansion. We identified fewer overall clones in the CD4 and
217 DPT populations when compared to the CD8 population. Furthermore, the top ten clones of both
218 the CD4 and DPT populations represent ~25% of the entire population while the top ten clones in
219 the CD8 population equal only half that number (Fig 3F, Supplemental Table 3).
220
221 To support our hypothesis that DPTs differentiate in response to xeno/allo-antigens and not as a
222 result of the lymphopenic environment found within allo-HSCT recipients and NSG mice, we
223 surveyed the phosphorylation status of several STAT proteins since they are downstream of a
224 variety of cytokine receptors, potentially offering insight into the development of DPTs.
225 Unfortunately, we could not identify any differences in the phosphorylation of STAT1, 3, 4 and 6
226 between the CD8 and DPT populations (Supplemental Fig 6A-B). Furthermore, the
227 transplantation of CD4 or CD8 T cells sorted from a previously transplanted xenogeneic GVHD
228 mouse into a naïve mouse did not result in the emergence of any DPTs (Fig 5D-F). This suggests
229 that the emergence of DPTs is not the result of lymphopenia or a xenogeneic microenvironment
230 but is instead the result of unknown activation events that occur early post-transplant in the CD8
231 T cell population.
232

233 Knowing that the transcriptome of DPT is unique compared to CD8 T cells and that transcription
234 factors were one of the functional analyses highlighted in the KEGG BRITE analysis, we further
235 investigated what transcription factors may be involved in the differentiation of DPT from the CD8
236 population. Interestingly, we observed that the transcriptional expression of the CD4 lineage
237 master transcription factor, THPOK (ZBTB7B) was significantly upregulated compared to CD8 T
238 cells (Fig 5G-H). DPTs also displayed significantly elevated levels of the CD8 lineage master
239 transcription factor, RUNX3, relative to CD4 T cells (Fig 5G-H). This dual expression of both CD4
240 and CD8 lineage master transcription factors was confirmed at the protein level by flow cytometry
241 which showed DPTs expressing an intermediate amount of each transcription factor relative to
242 their single positive T cell controls (Fig 5I-J). DPT also displayed differences in the polarizing
243 transcription factor T-bet (TBX21) which was increased relative to CD4 T cells but decreased
244 relative to CD8 T cells (Supplemental Fig 6C-E). There was also a small increase in the
245 expression of RORγt relative to CD8 T cells, a decrease in FOXP3 expression relative to CD4 T
246 cells and no difference in GATA3 expression (Supplemental Fig 6C-E).
247
248 **Differentiated DPTs are a metabolically active and unique T cell population**
249 To further explore DPT biology, we investigated their metabolic state relative to CD4 and CD8 T
250 cells. We analyzed sorted CD4, CD8 and DPTs from xenogeneic mice using a two-photon (2P)
251 autofluorescence imaging system (Fig 6A-E). This system is able to detect the autofluorescence
252 of NAD(P)H and FAD at a single cell resolution and use their ratios to determine the optical redox
253 ratio (ORR) of the cell population as a measurement of metabolic activity[56,57]. This analysis
254 revealed that the DPT population had elevated ORR, indicative of high metabolic activity (Fig 6A-
255 B). Furthermore, a random forest classifier trained to integrate the 10 metabolic parameters
256 imaged accurately identified the DPT population from CD4 and CD8 T cells (Fig 6C-E). This is
257 shown as a confusion matrix, ROC curve and a UMAP dimensionality reduction (Fig 6C-E).
258 Additional metabolic analysis using a Seahorse real-time metabolic analyzer independently

259 confirmed that DPTs have a higher ATP production rate than CD4 and CD8 T cells with the
260 increased ATP production primarily coming from glycolysis (Fig 6F). In addition to metabolic
261 differences, we also analyzed the T cell populations for evidence of “blasting”. Blasting is
262 characterized by increased cell size and is marker of cellular proliferation in T cells. The DPT
263 population displayed higher frequencies of the blasting phenotype relative to CD8 T cells in both
264 xenogeneic and clinical GVHD samples (Supplemental Fig 7).
265
266 **DPTs represent a GVHD-specific T cell population with little GVL activity**
267 To confirm the role of DPTs in the pathology of xenogeneic GVHD, we flow-sorted CD4, CD8 and
268 DPTs from GVHD mice and re-transplanted each population individually into naïve mice (Fig 7A).
269 Interestingly, only DPTs caused lethal xenogeneic GVHD (Fig 7B-C). DPTs expanded rapidly
270 after transplantation and had increased infiltration into the spleen, liver, and lungs relative to CD4
271 and CD8 T cells (Fig 7D-F). Mice transplanted with DPTs also exhibited high levels of human
272 IFNγ in their plasma compared to CD8 T cells (Fig 7G). To further investigate the secretome of
273 DPTs, we cultured human T cells from GVHD mice overnight with brefeldin A prior to intracellular
274 cytokine staining. DPTs secreted a diverse repertoire of cytokines including granzyme and
275 perforin, the inflammatory modulators IL-17A, IL-22 and GM-CSF as well as the activation
276 cytokines IFNγ and TNFα (Fig 6H-I, Supplemental Fig 8). These data highlight the extreme pro-
277 inflammatory state of DPTs and reveal this population to be the primary mediator of xenogeneic
278 GVHD pathology.
279
280 While we have shown evidence that DPTs are sufficient to mediate GVHD pathology, we next
281 wanted to determine if they can also mediate GVL activity against two human B-ALL
282 malignancies, NALM-6 and RS4;11. Human B-ALL cell lines were injected seven days prior to
283 the transplantation of CD4, CD8 or DPTs flow-sorted from GVHD mice (Fig 8A). Relative to control
284 mice only receiving the B-ALL cell line NALM-6, both flow-sorted CD4 and CD8 T cells were able

285 to prolong survival while DPTs provided no survival advantage (Fig 8B). The extended survival of
286 mice given flow-sorted CD4 and CD8 T cells was due to their ability to control the expansion of
287 NALM-6 as seen by IVIS and flow cytometry quantification of the number of NALM-6 cells in the
288 blood of these mice (Fig 8C-D). The failure of DPTs to prolong survival was not due to a lack of
289 cells within the mouse or a failure of activation as measured by IFNγ (Fig 8E-F). In fact, sorted
290 CD8 T cells were able to prolong survival even in the absence of detectable IFNγ suggesting they
291 maintain some GVL activity even without CD4 T cell help (Fig 8F). An in vitro cytotoxicity assay
292 of the flow-sorted T cell populations also revealed that DPTs had a three-fold lower capacity to
293 kill NALM-6 compared to flow-sorted CD4 and CD8 T cells (Fig 8G). Next, we determined if there
294 were any differences between flow sorted CD4 and CD8 T cells from a GVHD mouse and freshly
295 isolated CD4 and CD8 T cells from a healthy donor. We reveal that fresh CD4 and CD8 T cells
296 provided a similar survival advantage as before, highlighting that flow sorted CD4 and CD8 T cells
297 from GVHD mice do not lose their capacity to mediate GVL activity (Supplemental Fig 9). To
298 ensure this result is not specific to NALM-6, we tested flow-sorted CD4, CD8 and DPTs against
299 a second B-ALL cell line, RS4;11. DPTs also failed to protect against RS4;11 while flow-sorted
300 CD4 and CD8 T cells were able to prolong survival (Fig 8H-K). These results suggest that the
301 DPT population, which differentiates from the CD8 T cell population after transplant, may
302 represent a GVHD-specific T cell population with limited GVL activity against human B-ALL
303 malignancies.
304

305 **Discussion**

306 In this study, we identified five novel T cell specific predictive biomarkers of relapse and GVHD
307 which included a unique CD4/CD8 double positive T cell (DPT) population. Human DPTs originate
308 from the CD8 population after transplant through a currently unknown mechanism and are
309 transcriptionally, metabolically, and functionally distinct from CD4 and CD8 T cells. Furthermore,
310 we revealed that DPTs are sufficient for GVHD pathology when transplanted into naïve NSG mice

311 but possess little GVL activity against two human B-ALL cell lines. With DPTs also being identified
312 in other human chronic inflammatory diseases beyond GVHD, the molecular characterization of
313 DPTs in this manuscript may provide additional insight into the pathogenesis of these complex
314 diseases.
315
316 The identification of novel predictive biomarkers of allo-HSCT outcome is an important endeavor
317 that many groups have investigated in the past using serum analytes as biomarkers[17–19]. As such,
318 the direct investigation of T cells as a source of predictive biomarkers represents an exciting field
319 of biomarker research. Our results here suggest that the direct investigation of T cell metrics can
320 predict allo-HSCT outcomes early after transplant, independent of most pre-transplant prognostic
321 variables currently used in the clinic (Supplemental Table 1). While the use of T cell predictive
322 biomarkers will have to be validated in a larger multi-center study, this study highlights their
323 potential as a biomarker capable of predicting both relapse and GVHD after transplant.
324
325 To identify the five T cell predictive biomarkers in this study, we gated solely on the CD45RO$^+$ T
326 cell population. The gating on CD45RO$^+$ T cells is based on the knowledge that CD45RO is only
327 expressed on effector and memory T cells and the hypothesis that gating on this effector/memory
328 T cell population would provide additional sensitivity and reduce the “noise” in the system. With
329 the patient’s conditioning regimen eliminating or reducing their own T cell numbers to very low
330 levels, the CD45RO$^+$ T cell population most likely represents donor T cells from the graft. Thus,
331 we are using CD45RO as a marker to identify donor effector T cells that are activated against
332 either host or leukemia antigen. While we acknowledge that this gating strategy is not specific for
333 effector T cells, it allows us to remove naïve, non-reactive T cells that came from the donor graft
334 and naïve T cells generated de novo from hematopoiesis, which increases the sensitivity of our T
335 cell biomarkers.
336

337 Of the five T cell predictive biomarkers we identified, only DPTs lacked a verified biological
338 function. One recent manuscript which also identified DPTs in GVHD patients suggested that they
339 possess a regulatory function[44]. In our own analysis, we observed that an increase in the
340 percentage of DPTs was predictive of GVHD suggesting a positive correlation with pathology. In
341 our functional characterization of DPTs, we identified them as a highly activated T cell population
342 that expressed pro-inflammatory cytokines including IFNγ, TNFα, IL-17A, IL-22 and GM-CSF in
343 addition to perforin and granzyme (Fig 6H-I, Supplemental Fig 7). Furthermore, DPTs did not
344 display classical markers of exhaustion in our xenogeneic transplant model, with their expression
345 of PD-1, LAG3, TIGIT, TIM3 and CTLA4 all at or below CD4 or CD8 single-positive controls (Fig
346 4B-C, Supplemental Fig 5). This observation is further supported in our clinical observation study
347 where we show that DPTs express low levels of PD-1, TIGIT and lack the expression of LAG3
348 (Fig 4D-L). Our additional metabolic studies revealed they exist in an activated state that, when
349 re-transplanted in naïve mice, are sufficient to mediate GVHD pathology (Fig 7). These data
350 support our conclusion that DPTs represent a highly inflammatory T cell population that are
351 directly involved in pathology.
352
353 In addition to showing that DPTs are sufficient for lethal GVHD pathology, we also provide
354 evidence that they have limited GVL activity (Fig 7-8, Supplemental Fig 8). This surprising
355 observation is offset slightly by our inability to deplete DPTs without also depleting CD4 and/or
356 CD8 single-positive T cells. Currently, we have not identified a DPT specific marker uniquely
357 expressed by this population, which would have allowed us to confirm that the DPT population is
358 not required for GVL activity. Nevertheless, our experiments with flow sorted CD8 T cells from
359 GVHD mice which maintained GVL activity despite not being able to cause lethal xenogeneic
360 GVHD does provide supporting evidence that DPTs are not required for GVL activity (Fig 7 & 8).
361 While not conclusive, these data highlight the exciting possibility that a DPT-specific
362 immunotherapy may one day allow for the prevention of GVHD without inhibiting GVL activity.

363

364 With the CD4 T cell lineage have a well-established plasticity for different polarization states, we
365 were surprised to identify CD8 T cell as the origin of DPTs (Fig 5)[34,37–39]. Other than a CD8/FOXP3
366 regulatory T cell population, there are few other polarization states of CD8 T cells that have been
367 identified[42,43]. Furthermore, the master transcription factors of the CD8 and CD4 lineages, RUNX3
368 and THPOK respectively, are thought to negatively regulate each other[52]. While RUNX3 and
369 THPOK are both expressed in thymocytes during T cell development, mature T cells are thought
370 to be lineage restricted due to this process[52]. It was thus surprising that DPTs expressed both
371 RUNX3 and THPOK, both at the level of transcription and protein, via a currently unknown
372 mechanism. As such, additional studies will be required in the future to understand the signaling
373 and epigenetic mechanism(s) associated with this dual transcription factor expression (Fig 5).

374

375 Overall, this study uncovers the previously unknown origin and function of a human CD4/CD8
376 DPT population in GVHD that can also serve as a predictive biomarker of GVHD in adult allo-
377 HSCT patient samples. Metabolic, transcriptomic, and functional studies all identified DPTs as a
378 T cell population with distinct inflammatory properties relative single positive CD4 and CD8 T
379 cells. This highly inflammatory state resulted in lethal GVHD pathology when isolated DPTs were
380 transplanted into naïve NSG mice while CD4 and CD8 T cells populations, also isolated from
381 GVHD mice, failed to cause lethal pathology after re-transplantation. The DPT population though
382 could not control two human B-ALL cell lines, suggesting that the development of this population
383 from the CD8 T cell population might be dependent on chronic antigen stimulation from the host.
384 Future studies will need to explore the connection of DPTs with other human chronic inflammatory
385 disorders they have been identified in including rheumatoid arthritis, hepatitis B and C, β-
386 thalassemia, renal carcinomas, breast cancers and islet graft rejection[45–51]. In conclusion, DPTs
387 represent a unique T cell population whose presence should be directly investigated in other
388 human chronic inflammatory diseases.

389 **Methods**

390 *Isolation of Primary Human Cells.* Human peripheral blood was collected from healthy consenting
391 donors according to IRB protocol 2014-0806 (J.E.G.) and 2017-1070 (C.M.C). Leftover and de-
392 identified remnants of human bone marrow and G-CSF mobilized peripheral blood grafts used for
393 allo-HSCT procedures at our clinic were collected under IRB protocol 2016-0298 (P.H.). De-
394 identified human umbilical cord blood was collected from the Medical College of Wisconsin's cord
395 blood bank. All human blood samples were diluted 1:1 with leukocyte isolation buffer (PBS, 2mM
396 EDTA, 2% FBS) prior to ficoll density-gradient centrifugation (1100xg for 15 min with 0 brake).
397 When indicated, StemCell Technologies RosetteSep T cell, CD4 or CD8 enrichment kits were
398 used.

399

400 *Clinical Sample Collection.* All patients receiving an allo-HSCT at the University of Wisconsin-
401 Madison were prospectively enrolled between October 2020 and August 2021 on the minimal-
402 risk IRB protocol 2020-1490 (C.M.C.). A total of 35 patients were enrolled on this study. Eligible
403 patients had to receive post-transplant cyclophosphamide for GVHD prophylaxis at day +3/+4.
404 Conditioning regimen, HLA matching status, graft source and patient disease type were all non-
405 exclusion criteria for this study. Patients were divided into four respective categories based on
406 their allo-HSCT outcome: no GVHD, grade 1 GVHD, grade 2 GVHD or grade 3-4 GVHD. Patient
407 assignment into each respective GVHD category is based on their highest GVHD grade achieved
408 between day 0 and 100 after transplant. The development of GVHD after day 100 was not factored
409 into this analysis.

410

411 Excess blood from study patients was set aside after initial use and stored at 4ºC for 3-10 days
412 before processing and was never frozen. A total of 0.5mL of blood was aliquoted from each patient
413 collection tube for each flow cytometry test and centrifuged at 600xg for 4min at 4ºC. The cell
414 pellet was resuspended in 1.5mL of 1X RBC lysis buffer (BioLegend), vortexed and rested for

415 2min prior to washing with 1mL of PBS and centrifugation. Supernatant was disposed of and a
416 second round of RBC lysis was performed. Afterwards, the cell pellet was re-suspended in 1.5mL
417 of flow buffer (1X PBS + 2% FBS) and aliquoted into three flow cytometry tubes for staining.
418
419 *Transplantation of human cells into NSG Mice*. All human cells were washed and resuspended in
420 150µL/mouse of sterile 1X PBS prior to retro-orbital injection. Equal numbers of male and female
421 immunodeficient NSG (NOD.Cg-*Prkdc*^{scid} *Il2rg*^{tm1Wjl}/SzJ, Jackson Laboratories) between the ages
422 of 8-16 weeks of age were used for all experiments. All mice were weighed and monitored weekly
423 for visible signs of GVHD with a scoring system carried out as follows: 0 = no signs of GVHD; 1
424 = 2-5% weight loss; 2 = 6-9% weight loss; 3 = 10-14% weight loss; 4 = ≥ 15% weight loss. Blood
425 was regularly drawn at 1, 3, 6, 9- and 12-weeks post-transplant by retro-orbital bleeding. At time
426 of euthanasia, the spleen, one lobe of the liver, lungs and femur were regularly collected for further
427 processing.
428
429 *Flow Cytometry and Cell-Sorting.* All cells were stained in flow buffer (PBS, 10% FBS) prior to
430 quantification on a ThermoFisher Attune NxT Flow Cytometer and analysis on FlowJo V10.
431 Antibody clones include mCD45 (A20), ICOS (C398.4A), T-bet (4B10), LAG3 (11C3C65), FASL
432 (NOK-1), CD4 (OKT4), CD69 (FN50), OX40 (Ber-ACT35), CD27 (O323), pSTAT4 (p38), RORγt
433 (Q21-559), CD44 (BJ18), NKG2D (1D11), PD-1 (EH12.2H7), THPOK (ZFP-67), TIGIT
434 (A15153G), CD45RO (UCHL1), TIM3 (F38-2E2), pSTAT6 (A15137E), IL-22 (2G12A41), GATA3
435 (16E10A23), CD8α (RPA-T8), CD8β (SIDI8BEE), CD25 (BC96), 4-1BB (4B4-1), CD28 (CD28.2),
436 RUNX3 (SD0803), CTLA4 (BNI3), PanHLA (w6/32), CD3 (UCHT1). Visualization of cells was
437 complete using an ImageStream Mark II.
438
439 For cell sorting, cells were collected from the blood, spleen, liver and lungs of mice transplanted
440 with a lethal dose of PB-MNC approximately 4 weeks prior. Processed tissues were ficolled as

441 described above to obtain mononuclear cells. Human cells were isolated from the combined
442 mononuclear cells using StemCell Technologies EasySep Mouse/Human Chimera isolation kit.
443 Human cells were then stained in sterile PBS with the human CD4 (OKT4) and CD8β (SIDI8BEE)
444 antibodies prior to sorting on a BD FACSAria Cell Sorter. Cells were then maintained in cell culture
445 for 2-3 days prior to transplantation and/or expansion.
446
447 *Cell Lines and Cell Culture.* The human B-ALL line RS4;11 and NALM-6 were purchased from
448 ATCC and cultured using standard RPMI-10 media (RPMI base media, 10% FBS, 1X Pen/Strep,
449 1mM NEAA, 1X GlutaMAX). After flow sorting, isolated human CD4, CD8 and DPT populations
450 were expanded by co-culturing with a 10X dose of γ-irradiated (25Gy) human mononuclear cells
451 from a third-party donor with 5μg/mL of PHA in RPMI-10 media supplemented with 5ng/mL of
452 human IL-2 and IL-7. RPMI-10 media supplemented with IL-2 and IL-7 was added/changed
453 approximately every 3-4 days.
454
455 *RNA sequencing.* T cells from five GVHD mice were pooled prior to flow-sorting of the CD4, CD8
456 and DPTs. Pooled T cell populations were then split into three replicates for RNA isolation. All
457 RNA isolation and sequencing was performed by the Gene Expression Center at the University
458 of Wisconsin-Madison. RNA was isolated with Qiagen RNeasy kit prior to a quality control check
459 using an Agilent Bioanalyzer and NanoDrop One spectrophotometer. mRNA libraries were
460 prepared using the TruSeq stranded mRNA kit and sequenced on an Illumina NovaSeq 6000
461 platform to 30 million reads per sample. Sample reads were processed by the University of
462 Wisconsin Biotechnology Center.
463
464 *ELISAs.* Mouse blood samples were diluted with 50μL of 1X PBS prior to centrifugation with 60μL
465 of the diluted plasma stored at -20^{0}C. Plasma was further diluted 1:5 prior to ELISA with Assay
466 Buffer (PBS, 1mM Tween-20, 5% FBS). IFNγ ELISAs used the MD-1 clone for coating and a

467 biotinylated 4S.B3 clone for detection prior to visualization with a streptavidin-HRP antibody
468 (BioLegend).
469
470 *Two-photon lifetime imaging of NAD(P)H and FAD*
471 A custom-built inverted multiphoton microscope (Bruker Fluorescence Microscopy, Middleton, WI,
472 USA), was used to acquire fluorescence intensity and lifetime images. The equipment consists of
473 an ultrafast laser (Spectra Physics, Insight DSDual), an inverted microscope (Nikon, Eclipse Ti),
474 and a 40X water immersion (1.15 NA, Nikon) objective. NAD(P)H and FAD images were obtained
475 for the same field of view. FAD fluorescence was isolated using an emission bandpass filter of
476 550/100 nm and excitation wavelength of 890 nm. NAD(P)H fluorescence was isolated using an
477 emission bandpass filter of 440/80 nm and an excitation wavelength of 750 nm. Fluorescence
478 lifetime images were collected using time-correlated single-photon counting electronics (SPC-
479 150, Becker and Hickl, Brookline, MA, USA) and a GaAsP photomultiplier tube (H7422P-40,
480 Hamamatsu, Bridgewater, NJ, USA). 512x512 pixel images were obtained using a pixel dwell
481 time of 4.8 μs over 60 s total integration time. To guarantee adequate photon observations for
482 lifetime decay fits and no photobleaching, the photon count rates were maintained at 1–2 x 10^5
483 photons/s. The instrument response function was calculated from the second harmonic
484 generation of urea crystals excited at 900 nm. A Fluoresbrite YG microsphere (Polysciences Inc.,
485 Warrington, PA, USA) was imaged as a daily standard for fluorescence lifetime. The lifetime
486 decay curves for the YG microsphere standard were fit to a single exponential decay and the
487 fluorescence lifetime was measured to be 2.1 ns (n = 7), which is consistent with published values.
488 NAD(P)H and FAD intensity and lifetime images were analyzed using SPCImage software
489 (Becker &Hickl, Berlin, Germany) as described previously[58]. The fluorescence lifetime decay
490 curve was deconvolved with the instrument response function and fit to a two-component
491 exponential decay model at each pixel, $I(t) = \alpha_1 * e^{(-t/\tau_1)} + \alpha_2 * e^{(-t/\tau_2)} + C$, where I(t) represents
492 the fluorescence intensity at time t after the laser excitation pulse, α accounts for the fractional

493 contribution from each component, C represents the background light, and τ is the fluorescence
494 lifetime of each component. Since both NAD(P)H and FAD can exist in two conformational states,
495 bound, or unbound to enzymes, a two-component model was used. For NAD(P)H, the short (τ_1)
496 and long (τ_2) lifetime components correspond with the unbound and bound conformations,
497 respectively. The mean lifetime (τ_m) was calculated using $\tau_m = \alpha_{1*} \tau_1 + \alpha_{2*} \tau_2$, for both NAD(P)H and
498 FAD. The optical redox ratio was determined from the NAD(P)H and FAD intensity images as the
499 intensity of NAD(P)H / (NAD(P)H + FAD). Semi-automated cell segmentation was performed
500 using the cyto2 model in Cellpose, which resulted in whole-cell masks, followed by manual
501 inspection and mask corrections by a trained scientist. Using the masks, single cell features were
502 extracted including bi-exponential fit parameters (τ_1, τ_2, α_1, α_2) for NAD(P)H and FAD, NAD(P)H
503 τ_m, FAD τ_m, and the optical redox ratio. Features were calculated on a per-cell level by averaging
504 all the pixels across each cell. A minimum of 100 cells were analyzed per condition to obtain
505 statistically robust results.
506
507 *Metabolomic Assays.* ATP production rate was calculated from flow sorted CD4, CD8 and DPT
508 using an Agilent Seahorse XF Real-Time ATP Rate Assay Kit using a Seahorse XF/XFe96
509 analyzer and following the manufacturer's instructions.
510
511 *Bioluminescent Imaging.* A total of $1E^6$ luciferase positive NALM-6 cells were injected retro-
512 orbitally seven days prior to human T cell transplantation as described above. Luminescence
513 detection was gathered at the indicated times using an IVIS Spectrum In Vivo Imaging System
514 (PerkinElmer). Briefly, mice were anesthetized and intraperitoneally injected with 100μL of D-
515 luciferin at 30mg/mL with luminescence obtained approximately 15 minutes later.
516

517 *Statistics.* Graphs and statistical tests were completed using GraphPad Prism 6. All significance
518 tests were performed using either unpaired parametric (for linear data) or non-parametric (for
519 logarithmic data) t -tests. For the biomarker multivariate analysis, we used the multiplications of
520 the empirical cumulative distribution factor (ecdf) for each variable to achieve a combined score
521 with the R language. The AUC-ROC was used to determine the optimal direction of the exdf (< or
522 >) for each variable. Generalization performance was estimated using leave-one-out cross-
523 validation. For the RNA-seq analysis each fastq file is assessed for quality control issues and
524 trimmed to remove adapter sequences that were not removed by the initial demultiplexing. After
525 trimming and QC, the reads were aligned to the human genome using the splice-junction aware
526 read aligner STAR. The software package RSEM was used to generate normalized read counts
527 for each gene and its potential isoforms. Genes with very low expression, which would otherwise
528 reduce statistical power, were filtered out. The program EdgeR is then employed to perform
529 differential gene expression analysis.
530
531 *Study Approval.* All work involving human cells and tissues was performed in accordance with
532 IRB protocol 2014-0806 (C.M.C.). All animal work performed in accordance with UW-Madison
533 IACUC approved protocol number M005915 (C.M.C.).
534
535 **Author Contributions**
536 N.J.H., J.E.G., P.H. and C.M.C. designed the study; N.J.H., D.T. and J.R. performed experiments;
537 N.J.H., J.R., S.M. and E.C.G. analyzed the data; K.N., A.W.H., N.C., M.C.S. J.E.G. and P.H.
538 provided resources; N.J.H. and C.M.C. drafted the manuscript. All authors revised and approved
539 the manuscript.
540
541 **Grant Support**

542 The authors would like to thank the Clinical Laboratory team at UW-Health including Hugo Stoffel-
543 Rosales, Robin Rustad and Kaitlyn Walker for their help with sample collection, as well as the
544 the University of Wisconsin Carbone Cancer Center (UWCCC) Flow Cytometry Core Facility,
545 UWCCC Small Molecule Screening Facility, UWCCC Small Animal Imaging and Radiotherapy
546 Facility and the UWCCC Experimental Animal Pathology Laboratory, who are all supported by
547 NIH/NCI P30-CA014520. The authors also utilized the University of Wisconsin-Madison
548 Biotechnology Center Bioinformatics Core Facility for the analysis of RNA-sequencing data. This
549 work was supported in part by NIH/NIAID T32-AI125231 (N.J.H), NIH/NHLBI T32-HL07899
550 (N.J.H.), NIH/NCATS UL1-TR002373 (N.J.H), the Cormac Pediatric Leukemia Fellowship (N.J.H)
551 and the Stem Cell and Regenerative Medicine Center Fellowship (N.J.H.). Additional funding
552 includes NIH/NIAID R21-AI116007 (J.E.G.), NIH/NIAID R01-AI136500 (J.E.G.), St. Baldrick's-
553 Stand Up to Cancer Pediatric Dream Team Translational Research Grant SU2C-AACR-DT-27-
554 17 (C.M.C.), NIH/NCI R01-CA215461 (C.M.C.) and the MACC Fund (C.M.C). Stand Up to Cancer
555 is a division of the Entertainment Industry Foundation. Research grants are administered by the
556 American Association for Cancer Research, the scientific partner of SU2C. The contents of this
557 article do not necessarily reflect the views or policies of the Department of Health and Human
558 Services, nor does mention of trade names, commercial products, or organizations imply
559 endorsement by the US Government. None of these funding sources had any input in the study
560 design, analysis, manuscript preparation or decision to submit for publication.
561
562
563 **Disclosure of Conflicts of Interest**
564 C.M.C. reports honorarium from Bayer, Elephas Biosciences, Nektar Therapeutics and Novartis,
565 who had no input in the study design, analysis, manuscript preparation or decision to submit for
566 publication. The authors declare that no other relevant financial conflicts of interest exist.
567

568 **References**

569 1. D'Souza A, Fretham C, Lee SJ, et al. Current Use of and Trends in Hematopoietic Cell Transplantation
570 in the United States. *Biol Blood Marrow Transplant*. 2020;26(8):e177–e182.
571 2. Gooptu M, Romee R, St Martin A, et al. HLA-haploidentical vs matched unrelated donor transplants
572 with posttransplant cyclophosphamide-based prophylaxis. *Blood*. 2021;138(3):273–282.
573 3. Kanate AS, Majhail NS, Savani BN, et al. Indications for Hematopoietic Cell Transplantation and
574 Immune Effector Cell Therapy: Guidelines from the American Society for Transplantation and
575 Cellular Therapy. *Biol Blood Marrow Transplant*. 2020;26(7):1247–1256.
576 4. Martinez-Cibrian N, Zeiser R, Perez-Simon JA. Graft-versus-host disease prophylaxis:
577 Pathophysiology-based review on current approaches and future directions. *Blood Reviews*.
578 2020;100792.
579 5. Ciurea SO, Zhang M-J, Bacigalupo AA, et al. Haploidentical transplant with posttransplant
580 cyclophosphamide vs matched unrelated donor transplant for acute myeloid leukemia. *Blood*.
581 2015;126(8):1033–1040.
582 6. Battipaglia G, Labopin M, Kröger N, et al. Posttransplant cyclophosphamide vs antithymocyte
583 globulin in HLA-mismatched unrelated donor transplantation. *Blood*. 2019;134(11):892–899.
584 7. Blazar BR, Hill GR, Murphy WJ. Dissecting the biology of allogeneic HSCT to enhance the GvT effect
585 whilst minimizing GvHD. *Nat Rev Clin Oncol*. 2020;
586 8. Chang Y-J, Zhao X-Y, Huang X-J. Strategies for Enhancing and Preserving Anti-leukemia Effects
587 Without Aggravating Graft-Versus-Host Disease. *Front Immunol*. 2018;9:3041.
588 9. Reddy P, Maeda Y, Liu C, et al. A crucial role for antigen-presenting cells and alloantigen expression
589 in graft-versus-leukemia responses. *Nat. Med.* 2005;11(11):1244–1249.
590 10. Meurer T, Crivello P, Metzing M, et al. Permissive HLA-DPB1 mismatches in HCT depend on
591 immunopeptidome divergence and editing by HLA-DM. *Blood*. 2021;137(7):923–928.
592 11. Mayor NP, Wang T, Lee SJ, et al. Impact of Previously Unrecognized HLA Mismatches Using
593 Ultrahigh Resolution Typing in Unrelated Donor Hematopoietic Cell Transplantation. *JCO*.
594 2021;JCO.20.03643.
595 12. Petersdorf EW, Stevenson P, Bengtsson M, et al. HLA-B leader and survivorship after HLA-
596 mismatched unrelated donor transplantation. *Blood*. 2020;136(3):362–369.
597 13. Petersdorf EW, Gooley TA, Malkki M, et al. HLA-C expression levels define permissible mismatches
598 in hematopoietic cell transplantation. *Blood*. 2014;124(26):3996–4003.
599 14. Fuchs EJ, McCurdy SR, Solomon SR, et al. HLA informs risk predictions after haploidentical stem cell
600 transplantation with posttransplantation cyclophosphamide. *Blood*. 2022;139(10):1452–1468.
601 15. Wachsmuth LP, Patterson MT, Eckhaus MA, et al. Post-transplantation cyclophosphamide prevents
602 graft-versus-host disease by inducing alloreactive T cell dysfunction and suppression. *J Clin Invest*.
603 2019;129(6):2357–2373.
604 16. Nunes NS, Kanakry CG. Mechanisms of Graft-versus-Host Disease Prevention by Post-
605 transplantation Cyclophosphamide: An Evolving Understanding. *Front Immunol*. 2019;10:2668.
606 17. Paczesny S. Biomarkers for posttransplantation outcomes. *Blood*. 2018;131(20):2193–2204.
607 18. Chen S, Zeiser R. Novel Biomarkers for Outcome After Allogeneic Hematopoietic Stem Cell
608 Transplantation. *Front Immunol*. 2020;11:1854.
609 19. Adom D, Rowan C, Adeniyan T, Yang J, Paczesny S. Biomarkers for Allogeneic HCT Outcomes. *Front*
610 *Immunol*. 2020;11:673.
611 20. Srinagesh HK, Özbek U, Kapoor U, et al. The MAGIC algorithm probability is a validated response
612 biomarker of treatment of acute graft-versus-host disease. *Blood Adv*. 2019;3(23):4034–4042.

613 21. Hotta M, Satake A, Yoshimura H, et al. Elevation of Early Plasma Biomarkers in Patients with Clinical
614 Risk Factors Predicts Increased Nonrelapse Mortality after Allogeneic Hematopoietic Stem Cell
615 Transplantation. *Transplant Cell Ther*. 2021;27(8):660.e1-660.e8.
616 22. Rowan CM, Pike F, Cooke KR, et al. Assessment of ST2 for risk of death following graft-versus-host
617 disease in pediatric and adult age groups. *Blood*. 2020;135(17):1428–1437.
618 23. Major-Monfried H, Renteria AS, Pawarode A, et al. MAGIC biomarkers predict long-term outcomes
619 for steroid-resistant acute GVHD. *Blood*. 2018;131(25):2846–2855.
620 24. Zewde MG, Morales G, Gandhi I, et al. Evaluation of Elafin as a Prognostic Biomarker in Acute Graft-
621 versus-Host Disease. *Transplantation and Cellular Therapy, Official Publication of the American*
622 *Society for Transplantation and Cellular Therapy*. 2021;27(12):988.e1-988.e7.
623 25. Subburaj D, Ng B, Kariminia A, et al. Metabolomic identification of α-ketoglutaric acid elevation in
624 pediatric chronic graft-versus-host disease. *Blood*. 2022;139(2):287–299.
625 26. Inamoto Y, Martin PJ, Lee SJ, et al. Dickkopf-related protein 3 is a novel biomarker for chronic GVHD
626 after allogeneic hematopoietic cell transplantation. *Blood Adv*. 2020;4(11):2409–2417.
627 27. McCurdy SR, Radojcic V, Tsai H-L, et al. Signatures of GVHD and Relapse after Post-Transplant
628 Cyclophosphamide Revealed by Immune Profiling and Machine Learning. *Blood*.
629 2021;blood.2021013054.
630 28. Cruz CRY, Bo N, Bakoyannis G, et al. Antigen-specific T cell responses correlate with decreased
631 occurrence of acute GVHD in a multicenter contemporary cohort. *Bone Marrow Transplant*. 2021;
632 29. Podgorny PJ, Liu Y, Dharmani-Khan P, et al. Immune cell subset counts associated with graft-versus-
633 host disease. *Biol Blood Marrow Transplant*. 2014;20(4):450–462.
634 30. Magenau JM, Qin X, Tawara I, et al. Frequency of CD4+CD25hiFOXP3+ Regulatory T Cells Has
635 Diagnostic and Prognostic Value as a Biomarker for Acute Graft-versus-Host-Disease. *Biology of*
636 *Blood and Marrow Transplantation*. 2010;16(7):907–914.
637 31. Hess NJ, Brown ME, Capitini CM. GVHD Pathogenesis, Prevention and Treatment: Lessons From
638 Humanized Mouse Transplant Models. *Frontiers in Immunology*. 2021;12:3082.
639 32. Hill GR, Betts BC, Tkachev V, Kean LS, Blazar BR. Current Concepts and Advances in Graft-Versus-
640 Host Disease Immunology. *Annu Rev Immunol*. 2021;
641 33. Teshima T, Hill GR. The Pathophysiology and Treatment of Graft-Versus-Host Disease: Lessons
642 Learnt From Animal Models. *Front Immunol*. 2021;12:715424.
643 34. Piper C, Zhou V, Komorowski R, et al. Pathogenic Bhlhe40+ GM-CSF+ CD4+ T Cells Promote Indirect
644 Alloantigen Presentation in the GI Tract during GVHD. *Blood*. 2019;
645 35. Gartlan KH, Bommiasamy H, Paz K, et al. A critical role for donor-derived IL-22 in cutaneous chronic
646 GVHD. *Am. J. Transplant.* 2018;18(4):810–820.
647 36. Piper C, Hainstock E, Yin-Yuan C, et al. Single cell immune profiling reveals a developmentally
648 distinct CD4+ GM-CSF+ T cell lineage that induces GI tract GVHD. *Blood Adv*.
649 2022;bloodadvances.2021006084.
650 37. Park S, Griesenauer B, Jiang H, et al. Granzyme A-producing T helper cells are critical for acute graft-
651 versus-host disease. *JCI Insight*. 2020;
652 38. Hashimoto K, Kouno T, Ikawa T, et al. Single-cell transcriptomics reveals expansion of cytotoxic CD4
653 T cells in supercentenarians. *Proc Natl Acad Sci U S A*. 2019;116(48):24242–24251.
654 39. Mucida D, Husain MM, Muroi S, et al. Transcriptional reprogramming of mature $CD4^+$ helper T cells
655 generates distinct MHC class II-restricted cytotoxic T lymphocytes. *Nat. Immunol.* 2013;14(3):281–
656 289.
657 40. Takeuchi A, Saito T. CD4 CTL, a Cytotoxic Subset of CD4+ T Cells, Their Differentiation and Function.
658 *Front Immunol*. 2017;8:.
659 41. Dwyer GK, Mathews LR, Villegas JA, et al. IL-33 acts as a costimulatory signal to generate
660 alloreactive Th1 cells in graft-versus-host disease. *J Clin Invest*. 2022;e150927.

661 42. Agle K, Vincent BG, Piper C, et al. Bim regulates the survival and suppressive capability of CD8+
662 FOXP3+ regulatory T cells during murine GVHD. *Blood*. 2018;132(4):435–447.
663 43. Beres AJ, Haribhai D, Chadwick AC, et al. CD8+ Foxp3+ regulatory T cells are induced during graft-
664 versus-host disease and mitigate disease severity. *J. Immunol.* 2012;189(1):464–474.
665 44. Alhaj Hussen K, Michonneau D, Biajoux V, et al. CD4+CD8+ T-Lymphocytes in Xenogeneic and
666 Human Graft-versus-Host Disease. *Front Immunol*. 2020;11:579776.
667 45. Menard LC, Fischer P, Kakrecha B, et al. Renal Cell Carcinoma (RCC) Tumors Display Large Expansion
668 of Double Positive (DP) CD4+CD8+ T Cells With Expression of Exhaustion Markers. *Front Immunol*.
669 2018;9:2728.
670 46. Choi YJ, Park H-J, Park HJ, Jung KC, Lee J-I. CD4hiCD8low Double-Positive T Cells Are Associated with
671 Graft Rejection in a Nonhuman Primate Model of Islet Transplantation. *J Immunol Res*.
672 2018;2018:3861079.
673 47. Zahran AM, Saad K, Elsayh KI, Alblihed MA. Characterization of circulating CD4+ CD8+ double
674 positive and CD4- CD8- double negative T-lymphocyte in children with β-thalassemia major. *Int. J.*
675 *Hematol.* 2017;105(3):265–271.
676 48. Quandt D, Rothe K, Scholz R, Baerwald CW, Wagner U. Peripheral CD4CD8 double positive T cells
677 with a distinct helper cytokine profile are increased in rheumatoid arthritis. *PLoS ONE*.
678 2014;9(3):e93293.
679 49. Nascimbeni M, Pol S, Saunier B. Distinct CD4+CD8+ Double-Positive T Cells in the Blood and Liver of
680 Patients during Chronic Hepatitis B and C. *PLOS ONE*. 2011;6(5):e20145.
681 50. Desfrançois J, Derré L, Corvaisier M, et al. Increased frequency of nonconventional double positive
682 CD4CD8 αβ T cells in human breast pleural effusions. *International Journal of Cancer*.
683 2009;125(2):374–380.
684 51. Nascimbeni M, Shin E-C, Chiriboga L, Kleiner DE, Rehermann B. Peripheral CD4+CD8+ T cells are
685 differentiated effector memory cells with antiviral functions. *Blood*. 2004;104(2):478–486.
686 52. Egawa T. A Fateful Decision in the Thymus Controlled by the Transcription Factor ThPOK. *J.I.*
687 2021;206(9):1981–1982.
688 53. Overgaard NH, Jung J-W, Steptoe RJ, Wells JW. CD4+/CD8+ double-positive T cells: more than just a
689 developmental stage? *J. Leukoc. Biol.* 2015;97(1):31–38.
690 54. Hess NJ, Hudson AW, Hematti P, Gumperz JE. Early T Cell Activation Metrics Predict Graft-versus-
691 Host Disease in a Humanized Mouse Model of Hematopoietic Stem Cell Transplantation. *J. Immunol.*
692 2020;205(1):272–281.
693 55. Hess NJ, S Bharadwaj N, Bobeck EA, et al. iNKT cells coordinate immune pathways to enable
694 engraftment in nonconditioned hosts. *Life Sci Alliance*. 2021;4(7):.
695 56. Walsh AJ, Mueller K, Tweed K, et al. Classification of T-cell activation via autofluorescence lifetime
696 imaging. *Nat Biomed Eng*. 2021;5(1):77–88.
697 57. Samimi K, Contreras Guzman E, Trier SM, et al. Time-domain single photon-excited
698 autofluorescence lifetime for label-free detection of T cell activation. *Opt Lett*. 2021;46(9):2168–
699 2171.
700 58. Sharick JT, Walsh CM, Sprackling CM, et al. Metabolic Heterogeneity in Patient Tumor-Derived
701 Organoids by Primary Site and Drug Treatment. *Front Oncol*. 2020;10:553.
702

703 **Figure Legends**

704

705 **Figure 1. Post-transplant T cell metrics are predictive of allo-HSCT recipient disease**
706 **outcomes.**

707 (A) Schematic depicting the study outline. 35 allo-HSCT recipients had weekly blood samples
708 collected and processed without freezing. (B) Dot plots taken from five concatenated allo-HSCT
709 recipients who did not develop GVHD and those that developed ≥ grade 2 GVHD. Yellow box
710 indicates gating strategy for each T cell metric analyzed. (C-D) Samples collected between the
711 day 7 and 17 collection intervals were used for the analysis in (C) while samples collected
712 between the day 22 and 83 collection intervals were further normalized to each patient's date of
713 GVHD diagnosis (or day 54 for patient without GVHD) and used in (D). Each T cell metric was
714 analyzed in three binary tests shown in the bar graphs (left columns) with any tests showing
715 significance further analyzed by ROC (right columns). The mean, 95 confidence interval,
716 significance values and AUC are indicated in each graph. Each sample was treated independently
717 in these analyses. (E-F) T cell metrics exhibiting predictive value in each allo-HSCT outcome
718 were combined into a mutli-parameter ROC analysis. Analysis of the day 7-17 collection intervals
719 are in (E) and the day 22-83 collection intervals further normalized to GVHD diagnosis are shown
720 in (F).

721

722 **Figure 2. DPT develop after xenogeneic transplantation and are predictive of lethal GVHD**

723 (A) Kaplan-meier survival curve and flow plots of mice transplanted with PB-MNC and
724 representative dot plots from mouse blood at three weeks post-transplant corresponding to mice
725 that did not develop GVHD (blue) and those that developed lethal GVHD (red). (B) Representative
726 imagestream visualization of human T cells isolated from mouse blood three weeks post-
727 transplant. (C) Representative dot plots of mice transplanted with either PB-, MB-, BM- or CB-
728 MNC either at the time of euthanasia (GVHD mice, bottom) or at 12 weeks post-transplant (No

729 GVHD, top). Gating and percentage of DPTs are indicated by the red box. (D) Graphical
730 representation of the data from (C) representing >8 independent experiments. (E) Percentage of
731 DPTs in the blood of mice developing GVHD (red) or no GVHD (blue) at 1-, 3- and 6-weeks post-
732 transplant. (F-H) Data from (E) separated based on the graft source used for transplantation. (I)
733 ROC analysis of the data from (F). PB (peripheral blood), MB (G-CSF mobilized peripheral blood),
734 BM (bone marrow), CB (umbilical cord blood), MNC (mononuclear cells). Parametric t-test was
735 used to determine significance. * $p<0.05$, ** $p<0.01$, *** $p<0.001$
736
737 **Figure 3. The transcriptome of DPT is unique compared to CD4 and CD8 T cells**
738 (A) Venn diagram of the number of unique and shared differentially expressed genes among the
739 three comparisons indicated. (B) Unsupervised hierarchical clustering of the RNA-seq samples
740 using the computed Pearson correlation for each pair of samples and the Euclidean distances of
741 the correlation distances determined. (C-D) Volcano plots showing the number of differentially
742 expressed genes in the DPT:CD4 (C) and DPT:CD8 (D) comparisons using a cutoff of a ≥ 1 log
743 expression difference and a p-value of 0.01. (E) List of the 63 genes differentially expressed in
744 both the DPT:CD4 and DPT:CD8 comparisons. (F) TCR clonality analysis of the TRB gene
745 segments. Total number of unique TRB clones is indicated while the ten clones with the highest
746 frequency are colored in the pie graph.
747
748 **Figure 4. DPT Display A Transitional Expression Profile But With Reduced Expression of**
749 **Inhibitory Receptors**
750 (A) Imagestream visualization of DPTs expressing NKG2D. (B-C) Fold MFI of CD4 (green), DPTs
751 (red) and CD8 T cells (blue) expression of eight pro-inflammatory (B) and five inhibitory (C) co-
752 stimulatory receptors taken from GVHD mice at 3 weeks post-transplant. Data represents the
753 average Fold MFI of > five mice. (D-L) Analysis of nine pro-inflammatory (D-I) or inhibitory
754 receptors (J-L) on the surface of CD4, DPT or CD8 T cells from the allo-HSCT patient samples

755 collected as part of our observational study. Each dot represents the average Fold MFI of that
756 marker across all samples collected for one individual patient. Each minimum of 10 patients was
757 collected for each marker. Fold MFI = median fluorescent intensity of marker / isotype control.
758 Parametric t-test was used to determine significance. * $p<0.05$, ** $p<0.01$, *** $p<0.001$
759

760 **Figure 5. DPT differentiate from CD8 T cells after transplant and gain THPOK expression.**
761 (A) Unsupervised tSNE clustering of human T cells concatenated from five GVHD mice using a
762 9-color flow cytometry panel. (B-C) Freshly isolated CD3, CD4 and CD8 PB-Tc from a healthy
763 donor were transplanted into mice. Representative dot plots show the percentage of DPT in
764 mouse blood at three weeks post-transplant (B) with the percentage of DPT quantified in (C). (D)
765 Five mice transplanted with PB-MNC for 3 weeks were euthanized and the human cells isolated
766 from GVHD tissues prior to flow-sorting of the CD4 and CD8 T cells. (E-F) Dot plots and bar graph
767 of the percentage of DPT in the blood of mice re-transplanted with flow-sorted CD4 and CD8 T
768 cells three weeks post-transplant. Each dot represents an individual mouse. (G-J) Schematic
769 showing the standard expression dynamic of the transcription factors RUNX3 and THPOK in CD8
770 and CD4 T cells (G). (H) Table showing the fold change and p-value of RUNX3 and THPOK
771 (ZBTB7B) from our RNA-seq dataset. (I-J) Histograms and bar graphs of the Fold MFI of THPOK
772 and RUNX3 expression in CD4, DPT and CD8 T cells from GVHD mice. Fold MFI = median
773 fluorescent intensity of marker / isotype control. Parametric t-test was used to determine
774 significance. * $p<0.05$, ** $p<0.01$, *** $p<0.001$
775

776 **Figure 6. DPT cells exhibit a metabolically unique signature from other T cells.**
777 (A) Representative images from live-cell imaging of NAD(P)H τm (0.5-1.5 ns), FAD τm (0.3-1.3
778 ns), and optical redox ratio images (shown are 6 image sets of 24 sets) from flow-sorted CD4,
779 CD8 and DPT from GVHD mice. All cells were cultured for 48hrs but activated cells were also
780 stimulated with CD3/CD28/CD2 12hrs prior to imaging. Scale bar at top left, 25 μm. (B) Scatter

781 plots of the optical redox ratio (NAD(P)H / (NAD(P)H + FAD), mean NAD(P)H lifetime in ns, mean
782 FAD lifetime in ns, % unbound NAD(P)H, % protein-bound FAD. Each dot represents a single cell
783 with mean at center and error bars representing 1 standard deviation. (C-D) Confusion matrix (C)
784 and ROC curve (D) of a random forest classifier trained on the 10 OMI parameters (NAD(P)H and
785 FAD τ1, τ2, α1, α2, τm) for classification of DPT cells from CD4 and CD8 T cells. (E) UMAP
786 dimensionality reduction analysis of OMI parameter results (τ1, τ2, α1, α2, τm) for both NAD(P)H
787 and FAD. (F) Seahorse analysis of the ATP production rate of flow-sorted CD4, DPT and CD8 T
788 cells. Parametric t-test was used to determine significance. * $p<0.05$, ** $p<0.01$, *** $p<0.001$, ****
789 $p<0.0001$.Cell counts for each population: 365 CD4 ctrl, 598CD4 act, 199 DPT ctrl, 155 DPT act,
790 103 CD8 ctrl, 119 CD8 act.
791
792 **Figure 7. DPTs are sufficient to mediate GVHD pathology.**
793 (A) Schematic of experimental design. (B-G) Kaplan-meier survival curve (B) and GVHD score
794 (C) of mice transplanted with flow-sorted CD4, DPT and CD8 T cells from five pooled GVHD mice.
795 (D) Quantification of T cells numbers in GVHD target organs at time of euthanasia. Representative
796 H&E staining of liver and lung sections from transplanted mice (E) and histological scoring (F).
797 (G) Quantification of IFNγ levels in the plasma of transplanted mice. (H-I) Splenic T cells from
798 GVHD mice were cultured overnight with either Brefeldin A alone or Brefeldin A with a 4-hour
799 PMA/ionomycin stimulation prior to ICS staining of the indicated cytokine. Data is compiled from
800 4-13 mice. Non-parametric t-tests were used for determining significance between T cell numbers
801 while parametric t-tests were used for all other analyses. * $p<0.05$, ** $p<0.01$, *** $p<0.001$
802
803 **Figure 8. DPTs have limited GVL activity relative to CD4 and CD8 T cells.**
804 (A) Schematic of experiment design. The B-ALL cell line NALM-6 was transplanted for (B-G) and
805 RS4;11 for (H-K). (B-G) Kaplan-meier survival curve (B), IVIS images (C), quantification of the
806 number of NALM-6 (D) and T cells (E) in the blood and IFNγ levels in the plasma (F). (G) NALM-

807 6 cells pre-loaded with Calcein dye were co-cultured with flow-sorted CD4, DPT and CD8 T cells
808 for four hours and supernatants quantified for the presence of calcein. Data is expressed relative
809 to a max kill condition using Triton-X. (H-K) Kaplan-meier survival curve (H), quantification of
810 RS4;11 (I) and T cells in the blood (J) and IFNγ in the plasma (K) of mice transplanted with
811 RS4;11. Non-parametric t-tests were used to determine significance for the quantification of B-
812 ALL and T cell numbers while parametric t-tests were used for all other analyses. * $p<0.05$, **
813 $p<0.01$

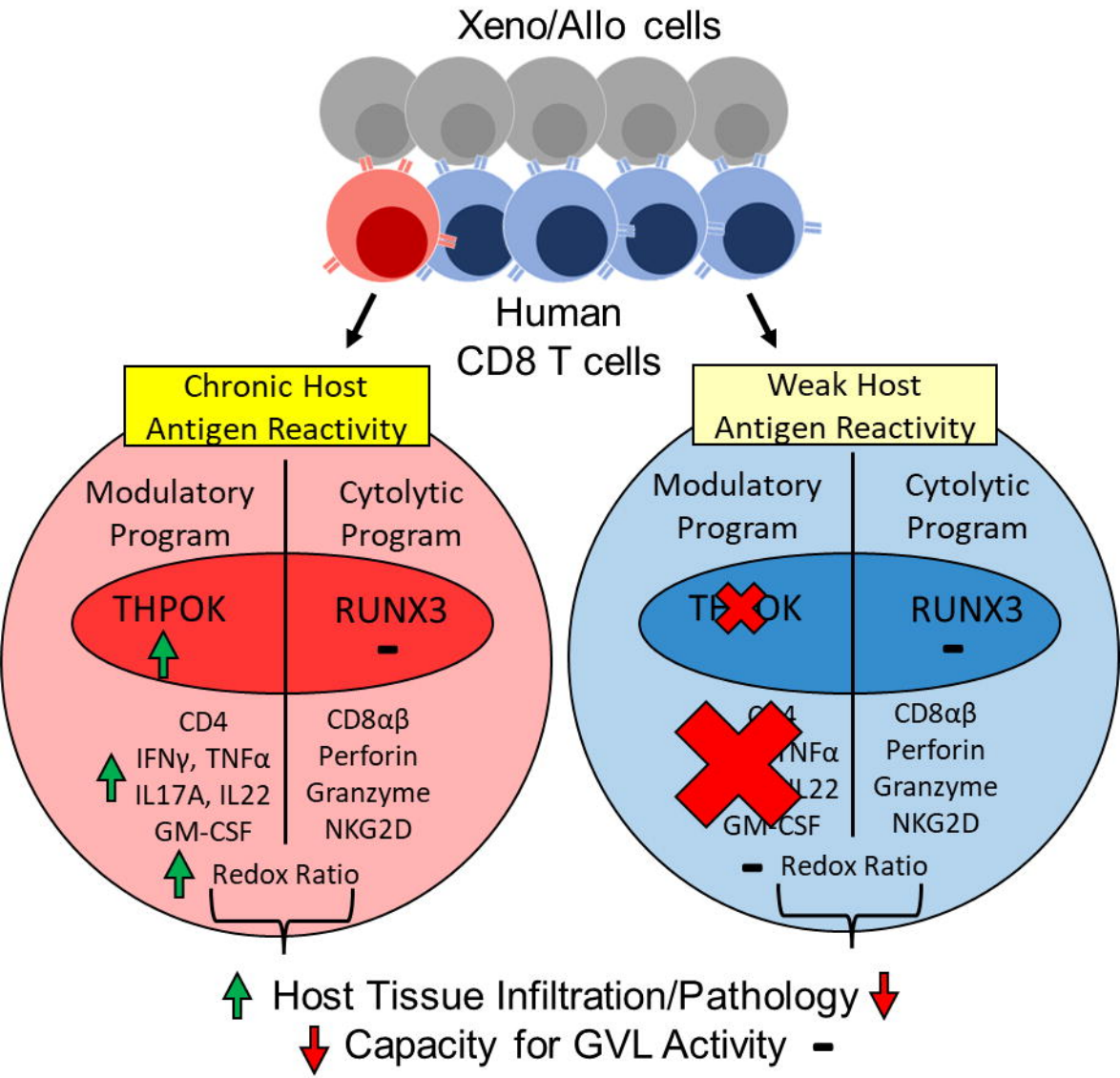
Xeno/Allo cells
Human
CD8 T cells
Chronic Host
Antigen Reactivity
Modulatory
Program
Cytolytic
Program
THPOK
RUNX3
CD4
IFNγ, TNFα
IL17A, IL22
GM-CSF
CD8αβ
Perforin
Granzyme
NKG2D
Redox Ratio
Weak Host
Antigen Reactivity
Modulatory
Program
Cytolytic
Program
RUNX3
CD8αβ
Perforin
Granzyme
NKG2D
Redox Ratio
Host Tissue Infiltration/Pathology
Capacity for GVL Activity

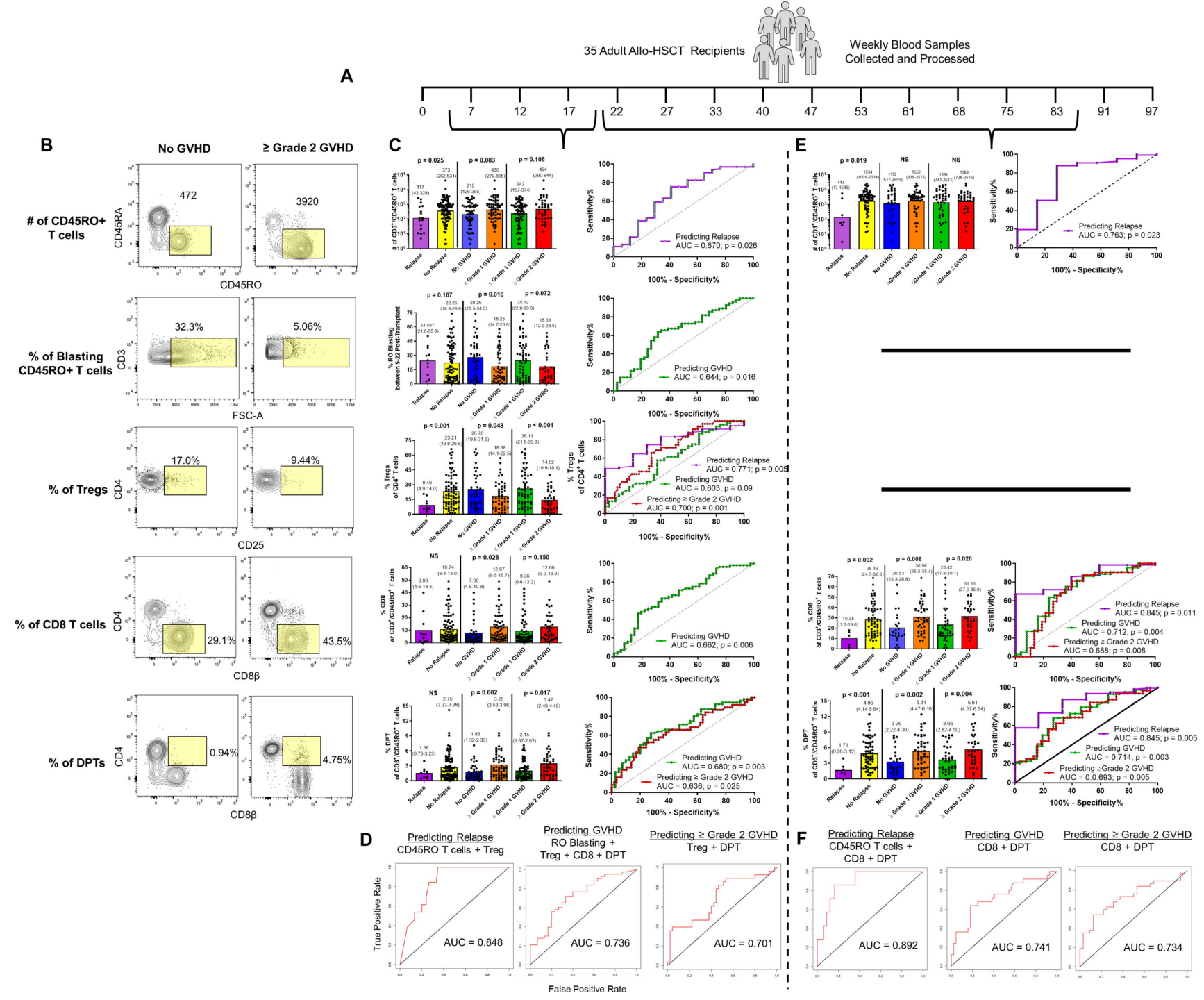
A
35 Adult Allo-HSCT Recipients
Weekly Blood Samples Collected and Processed
0 7 12 17 22 27 33 40 47 53 61 68 75 83 91 97
B
No GVHD
≥ Grade 2 GVHD
# of CD45RO+ T cells
472
3920
CD45RA
CD45RO
% of Blasting CD45RO+ T cells
32.3%
5.06%
CD3
FSC-A
% of Tregs
17.0%
9.44%
CD4
CD25
% of CD8 T cells
29.1%
43.5%
CD8β
% of DPTs
0.94%
4.75%
C
p = 0.025
p = 0.083
p = 0.106
Predicting Relapse
AUC = 0.670; p = 0.026
p = 0.167
p = 0.010
p = 0.072
Predicting GVHD
AUC = 0.644; p = 0.016
p < 0.001
p = 0.048
p < 0.001
Predicting Relapse
AUC = 0.771; p = 0.005
Predicting GVHD
AUC = 0.603; p = 0.09
Predicting ≥ Grade 2 GVHD
AUC = 0.700; p = 0.001
NS
p = 0.028
p = 0.150
Predicting GVHD
AUC = 0.662; p = 0.006
NS
p = 0.002
p = 0.017
Predicting GVHD
AUC = 0.680; p = 0.003
Predicting ≥ Grade 2 GVHD
AUC = 0.636; p = 0.025
Relapse
No Relapse
No GVHD
≥ Grade 1 GVHD
≤ Grade 1 GVHD
≥ Grade 2 GVHD
Sensitivity%
100% - Specificity%
E
p = 0.019
NS
NS
Predicting Relapse
AUC = 0.763; p = 0.023
p = 0.002
p = 0.008
p = 0.026
Predicting Relapse
AUC = 0.845; p = 0.011
Predicting GVHD
AUC = 0.712; p = 0.004
Predicting ≥ Grade 2 GVHD
AUC = 0.688; p = 0.008
p < 0.001
p = 0.002
p = 0.004
Predicting Relapse
AUC = 0.845; p = 0.005
Predicting GVHD
AUC = 0.714; p = 0.003
Predicting ≥ Grade 2 GVHD
AUC = 0.0.693; p = 0.005
D
Predicting Relapse
CD45RO T cells + Treg
Predicting GVHD
RO Blasting + Treg + CD8 + DPT
Predicting ≥ Grade 2 GVHD
Treg + DPT
True Positive Rate
False Positive Rate
AUC = 0.848
AUC = 0.736
AUC = 0.701
F
Predicting Relapse
CD45RO T cells + CD8 + DPT
Predicting GVHD
CD8 + DPT
Predicting ≥ Grade 2 GVHD
CD8 + DPT
AUC = 0.892
AUC = 0.741
AUC = 0.734

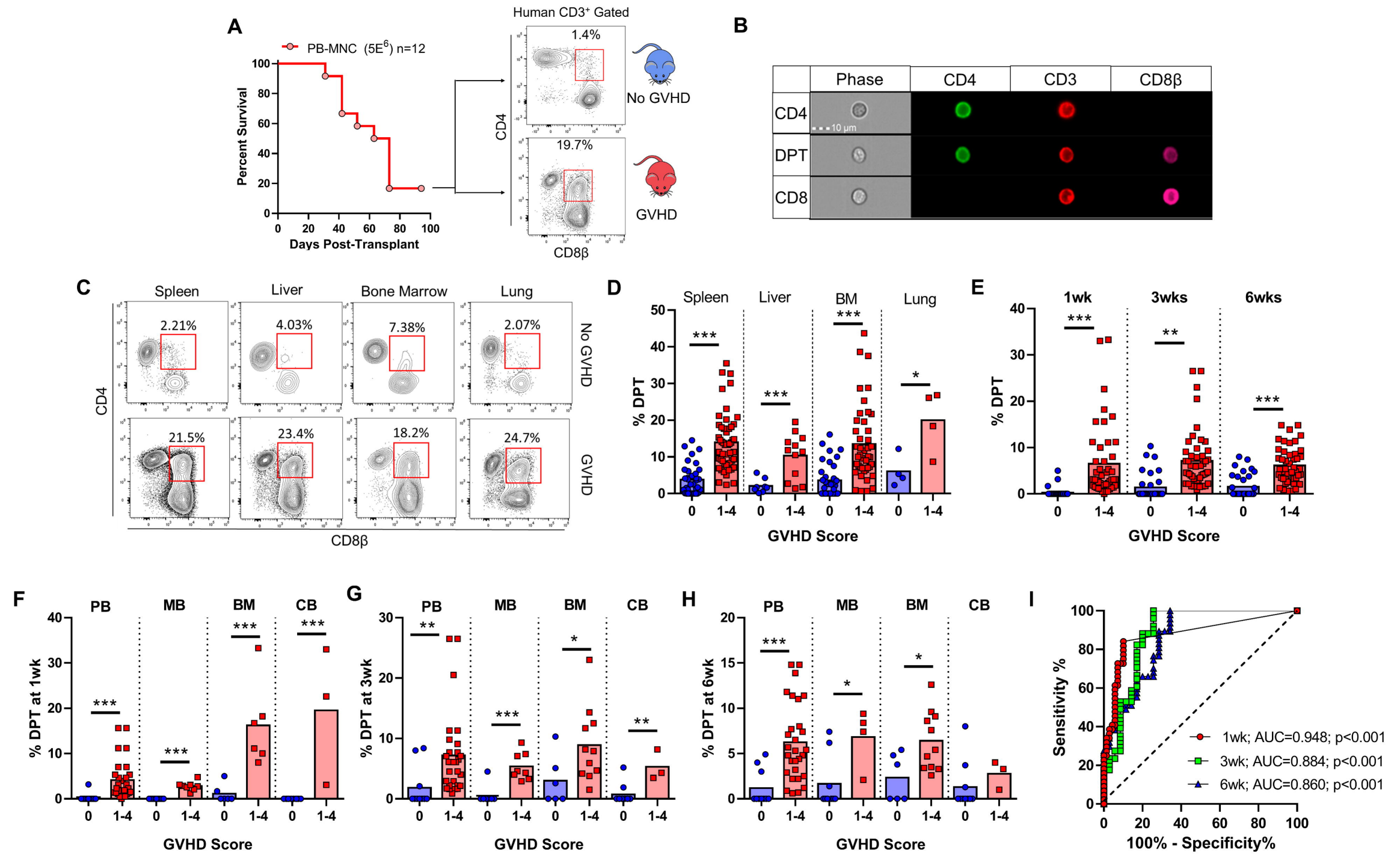
A
PB-MNC (5E6) n=12
Percent Survival
Days Post-Transplant
Human CD3+ Gated
1.4%
19.7%
CD4
CD8β
No GVHD
GVHD
B
Phase
CD4
CD3
CD8β
DPT
CD8
10 µm
C
Spleen
Liver
Bone Marrow
Lung
2.21%
4.03%
7.38%
2.07%
21.5%
23.4%
18.2%
24.7%
No GVHD
GVHD
D
% DPT
GVHD Score
E
1wk
3wks
6wks
F
PB
MB
BM
CB
% DPT at 1wk
G
% DPT at 3wk
H
% DPT at 6wk
I
Sensitivity %
100% - Specificity%
1wk; AUC=0.948; p<0.001
3wk; AUC=0.884; p<0.001
6wk; AUC=0.860; p<0.001

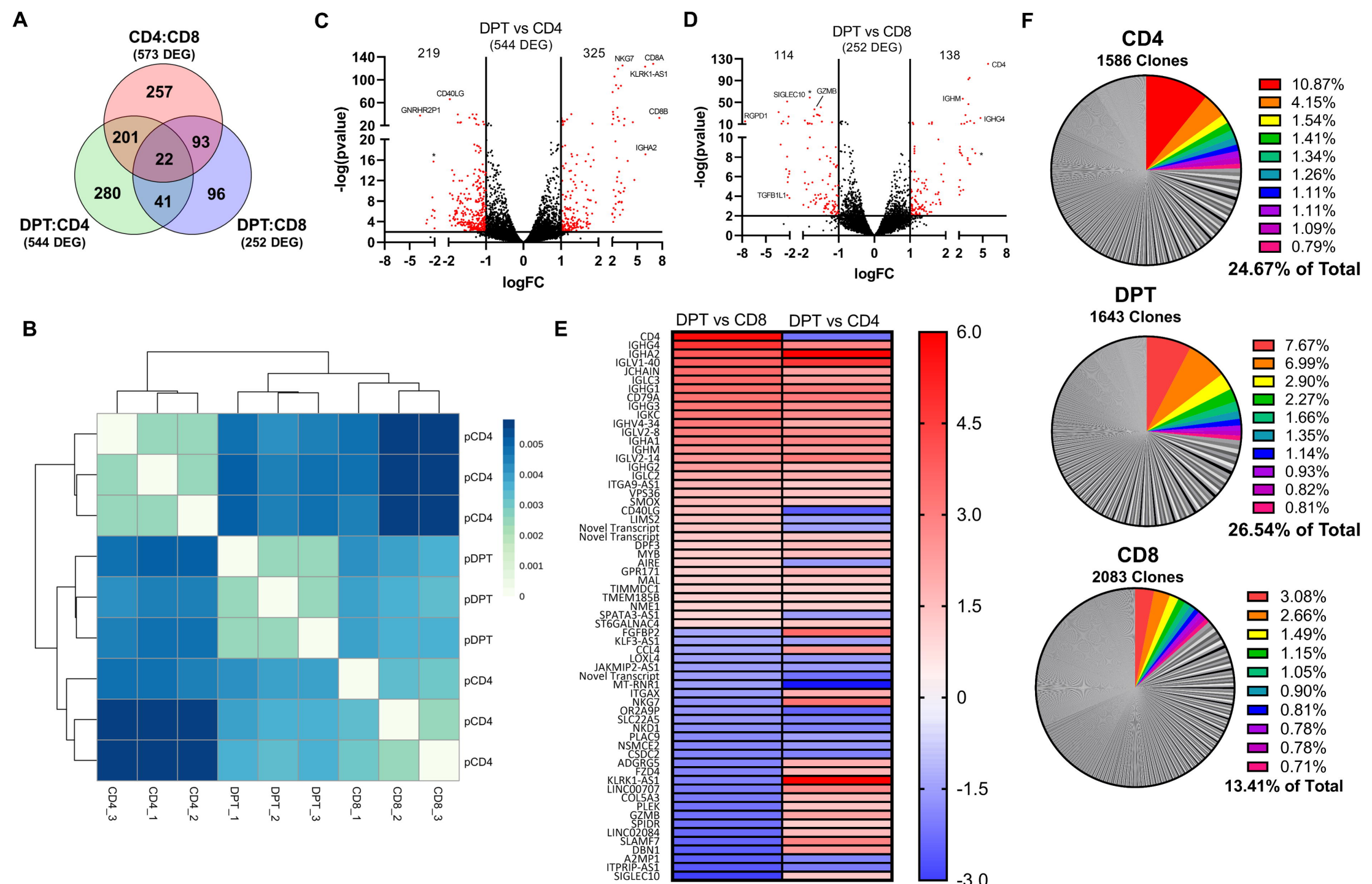
A
CD4:CD8
(573 DEG)
257
201
93
22
280
41
96
DPT:CD4
(544 DEG)
DPT:CD8
(252 DEG)
C
DPT vs CD4
(544 DEG)
219
325
NKG7
CD8A
KLRK1-AS1
CD40LG
GNRHR2P1
CD8B
IGHA2
-log(pvalue)
logFC
D
DPT vs CD8
(252 DEG)
114
138
CD4
SIGLEC10
GZMB
IGHM
IGHG4
RGPD1
TGFB1L1
-log(pvalue)
logFC
F
CD4
1586 Clones
10.87%
4.15%
1.54%
1.41%
1.34%
1.26%
1.11%
1.11%
1.09%
0.79%
24.67% of Total
DPT
1643 Clones
7.67%
6.99%
2.90%
2.27%
1.66%
1.35%
1.14%
0.93%
0.82%
0.81%
26.54% of Total
CD8
2083 Clones
3.08%
2.66%
1.49%
1.15%
1.05%
0.90%
0.81%
0.78%
0.78%
0.71%
13.41% of Total
B
pCD4
pDPT
CD4_3
CD4_1
CD4_2
DPT_1
DPT_2
DPT_3
CD8_1
CD8_2
CD8_3
E
DPT vs CD8
DPT vs CD4
CD4
IGHG4
IGHA2
IGLV1-40
JCHAIN
IGLC3
IGHG1
CD79A
IGHG3
IGKC
IGHV4-34
IGLV2-8
IGHA1
IGHM
IGLV2-14
IGHG2
IGLC2
ITGA9-AS1
VPS36
SMOX
CD40LG
LIMS2
Novel Transcript
Novel Transcript
DPF3
MYB
AIRE
GPR171
MAL
TIMMDC1
TMEM185B
NME1
SPATA3-AS1
ST6GALNAC4
FGFBP2
KLF3-AS1
CCL4
LOXL4
JAKMIP2-AS1
Novel Transcript
MT-RNR1
ITGAX
NKG7
OR2A9P
SLC22A5
NKD1
PLAC9
NSMCE2
CSDC2
ADGRG5
FZD4
KLRK1-AS1
LINC00707
COL5A3
PLEK
GZMB
SPIDR
LINC02084
SLAMF7
DBN1
A2MP1
ITPRIP-AS1
SIGLEC10
6.0
4.5
3.0
1.5
0
-1.5
-3.0

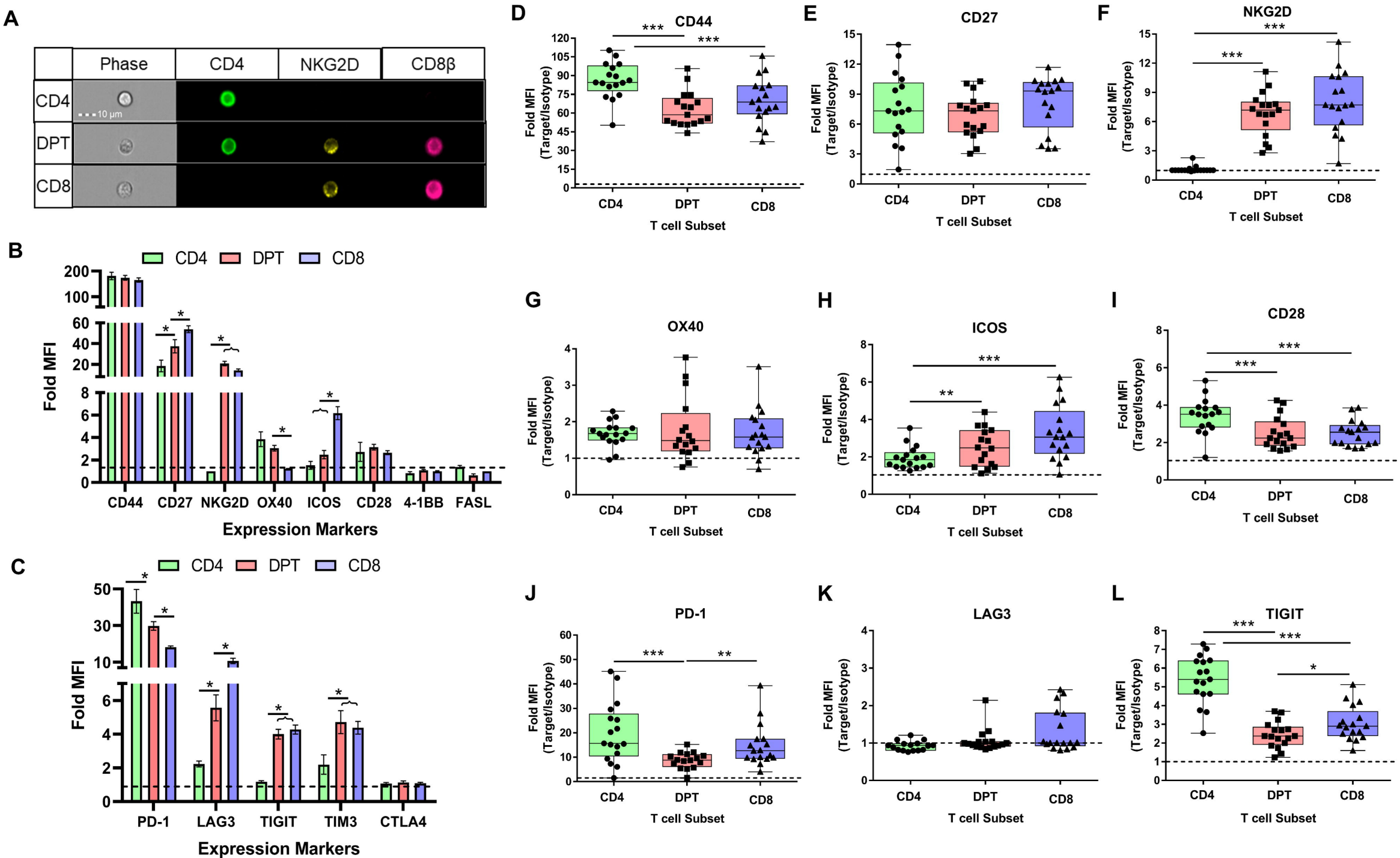
A
Phase
CD4
NKG2D
CD8β
CD4
DPT
CD8
10 µm
B
CD4
DPT
CD8
Fold MFI
CD44
CD27
NKG2D
OX40
ICOS
CD28
4-1BB
FASL
Expression Markers
C
CD4
DPT
CD8
Fold MFI
PD-1
LAG3
TIGIT
TIM3
CTLA4
Expression Markers
D
CD44
E
CD27
F
NKG2D
G
OX40
H
ICOS
I
CD28
J
PD-1
K
LAG3
L
TIGIT
Fold MFI (Target/Isotype)
T cell Subset

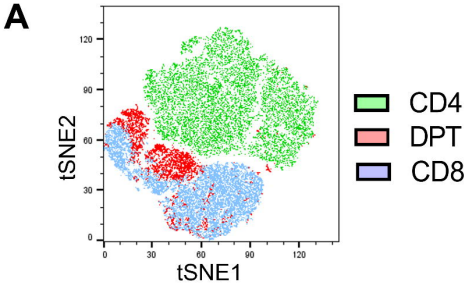

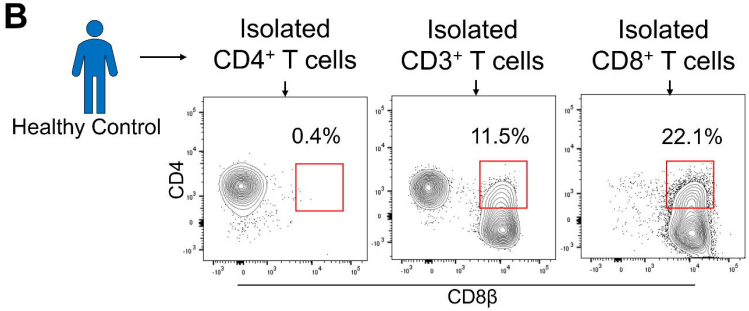

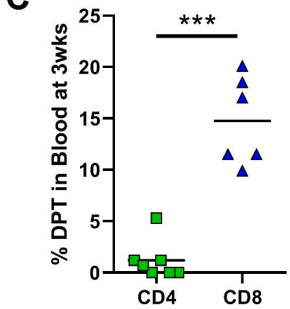

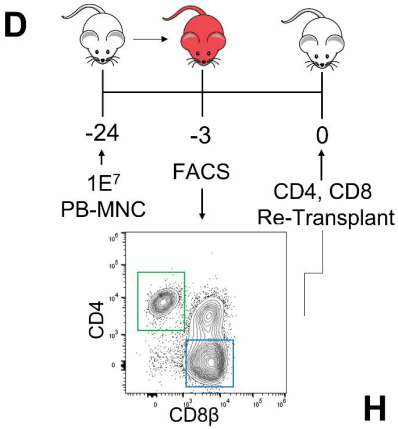

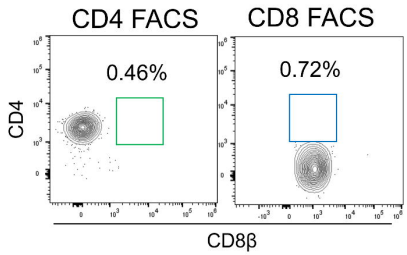

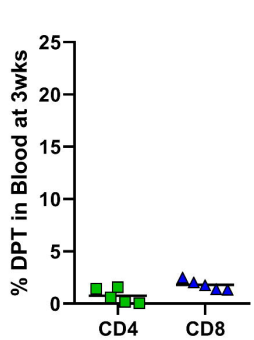

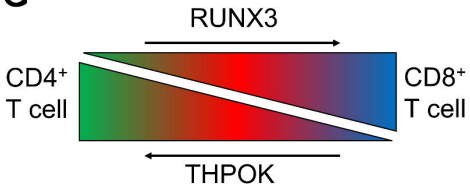

H

Comparison	Gene Name (Protein)	Fold Change	p-value
DPT:CD4	RUNX3	**0.728**	**1.15E^{-7}**
	ZBTB7B (THPOK)	-0.142	0.21
DPT:CD8	RUNX3	-.0188	0.163
	ZBTB7B (THPOK)	**1.093**	**8.14E^{11}**

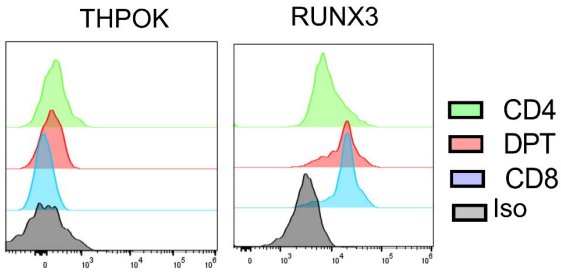

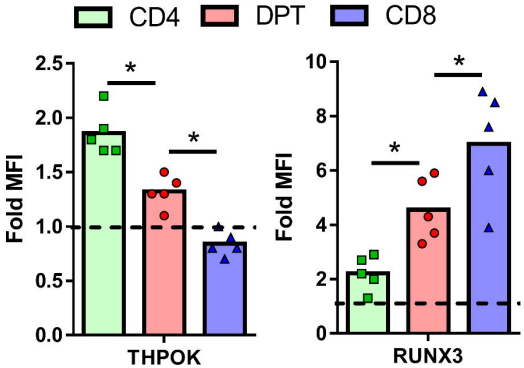

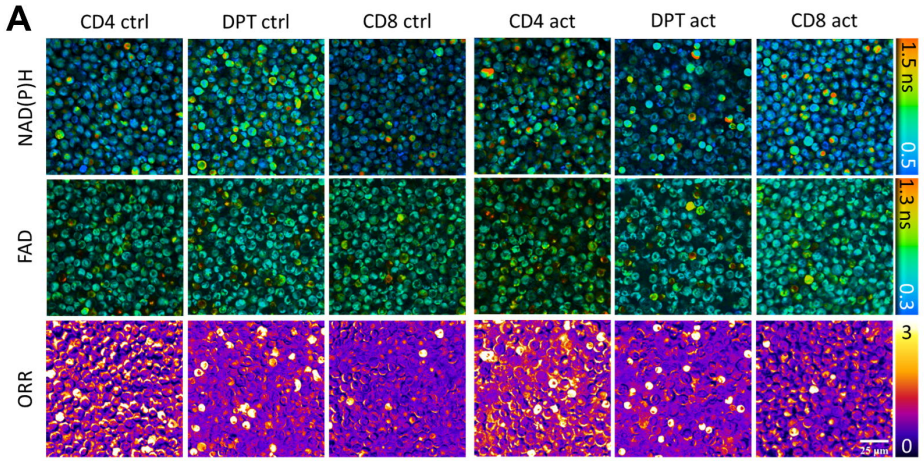

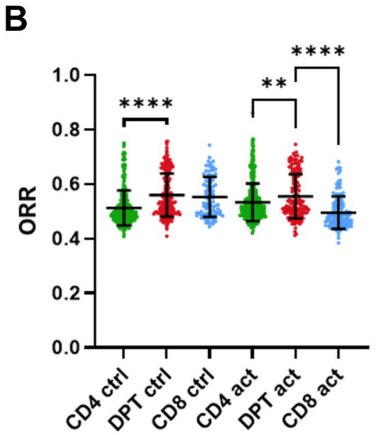

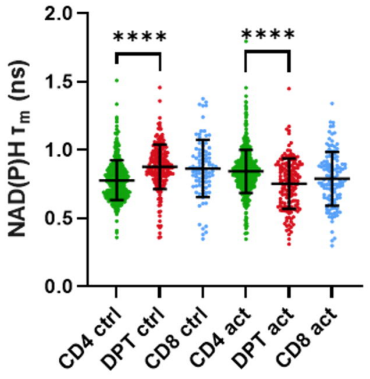

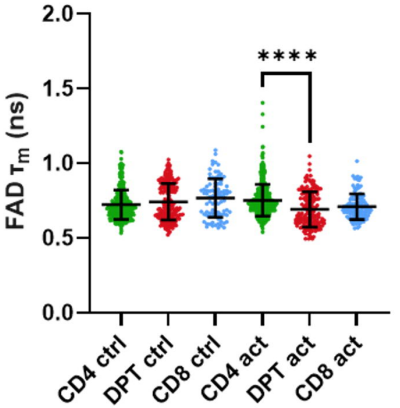

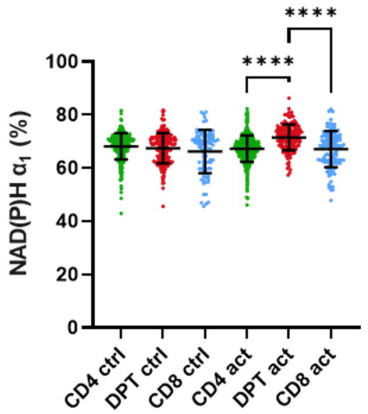

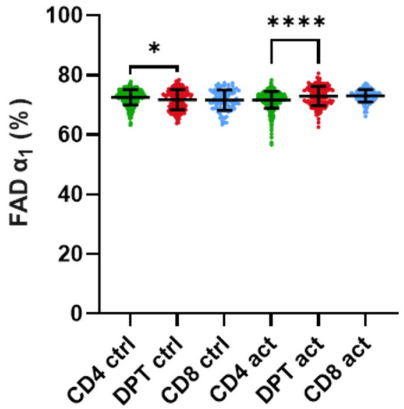

C

Random forest		Predicted Condition	
		DPT	CD4 & CD8
Actual Condition	DPT	85.64	29.17
	CD4 & CD8	14.36	70.83

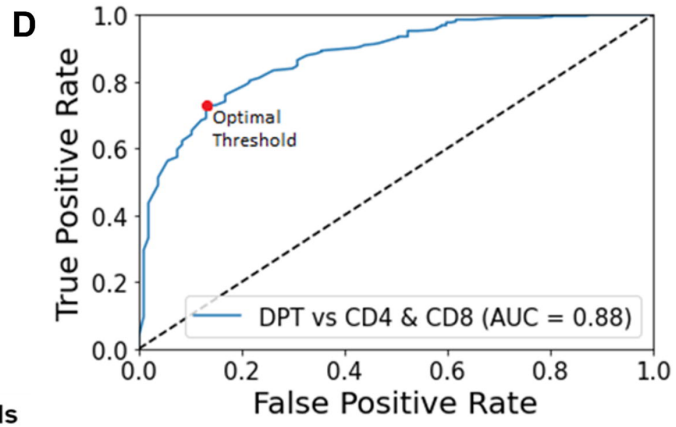

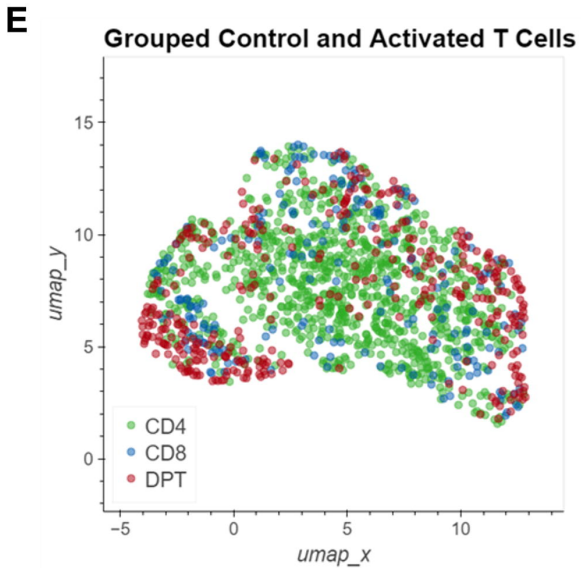

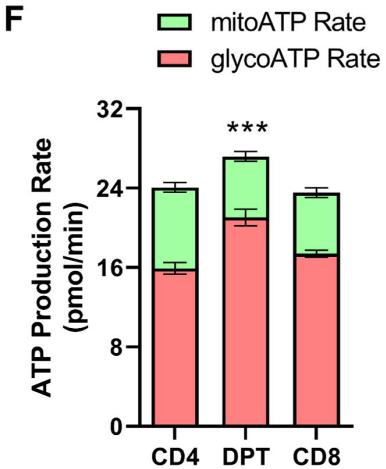

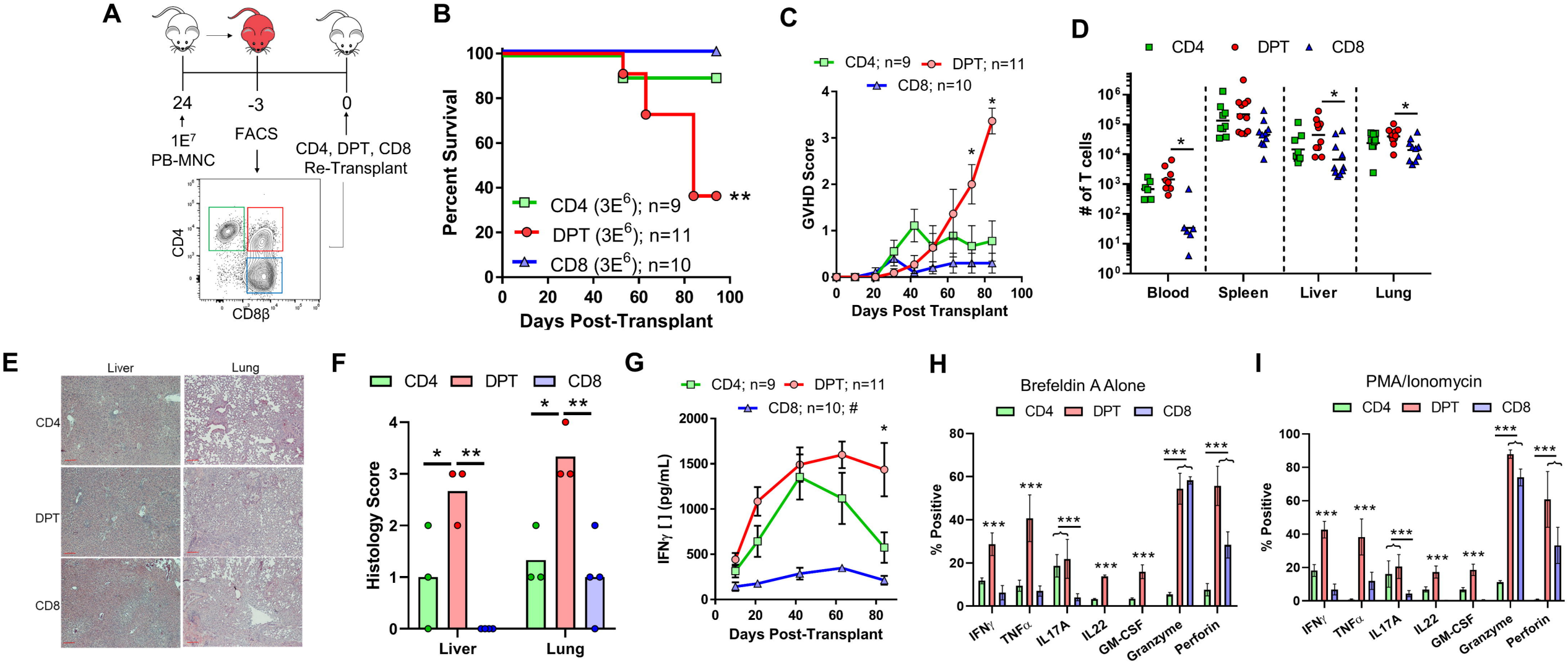
A
24
-3
0
1E7
PB-MNC
FACS
CD4, DPT, CD8
Re-Transplant
CD4
CD8β
B
Percent Survival
Days Post-Transplant
CD4 (3E6); n=9
DPT (3E6); n=11
CD8 (3E6); n=10
**
C
CD4; n=9
DPT; n=11
CD8; n=10
GVHD Score
Days Post Transplant
D
CD4
DPT
CD8
# of T cells
Blood
Spleen
Liver
Lung
E
Liver
Lung
CD4
DPT
CD8
F
CD4
DPT
CD8
Histology Score
Liver
Lung
G
CD4; n=9
DPT; n=11
CD8; n=10; #
IFNγ [ ] (pg/mL)
Days Post-Transplant
H
Brefeldin A Alone
CD4
DPT
CD8
% Positive
IFNγ
TNFα
IL17A
IL22
GM-CSF
Granzyme
Perforin
I
PMA/Ionomycin
CD4
DPT
CD8
% Positive
IFNγ
TNFα
IL17A
IL22
GM-CSF
Granzyme
Perforin

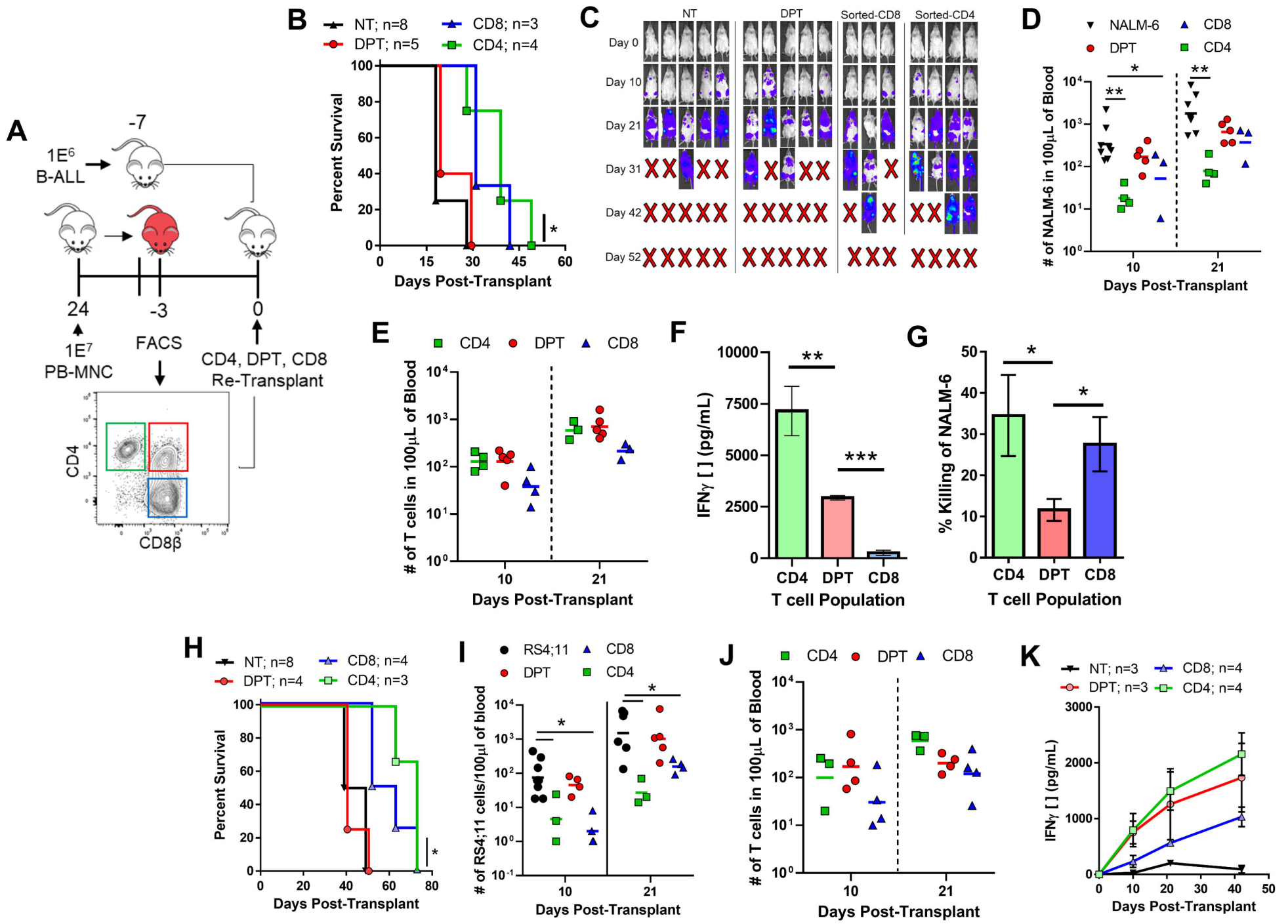
A
-7
1E6
B-ALL
24
-3
0
1E7
PB-MNC
FACS
CD4, DPT, CD8
Re-Transplant
CD4
CD8β
B
NT; n=8
DPT; n=5
CD8; n=3
CD4; n=4
Percent Survival
Days Post-Transplant
C
NT
DPT
Sorted-CD8
Sorted-CD4
Day 0
Day 10
Day 21
Day 31
Day 42
Day 52
D
NALM-6
DPT
CD8
CD4
# of NALM-6 in 100μL of Blood
Days Post-Transplant
E
CD4
DPT
CD8
# of T cells in 100μL of Blood
Days Post-Transplant
F
IFNγ [ ] (pg/mL)
CD4
DPT
CD8
T cell Population
G
% Killing of NALM-6
CD4
DPT
CD8
T cell Population
H
NT; n=8
DPT; n=4
CD8; n=4
CD4; n=3
Percent Survival
Days Post-Transplant
I
RS4;11
DPT
CD8
CD4
# of RS4;11 cells/100μl of blood
Days Post-Transplant
J
CD4
DPT
CD8
# of T cells in 100μL of Blood
Days Post-Transplant
K
NT; n=3
DPT; n=3
CD8; n=4
CD4; n=4
IFNγ [ ] (pg/mL)
Days Post-Transplant